HHS Public Access

Author manuscript

Cell Rep. Author manuscript; available in PMC 2020 July 19.

Published in final edited form as:

Cell Rep. 2020 May 26; 31(8): 107679. doi:10.1016/j.celrep.2020.107679.

Targeting Lymph Node Niches Enhances Type 1 Immune Responses to Immunization

Jeffrey Lian[1,2], **Aleksandra J. Ozga**[1], **Caroline L. Sokol**[1], **Andrew D. Luster**[1,2,3,*]

[1]Center for Immunology & Inflammatory Diseases, Division of Rheumatology, Allergy & Immunology, Massachusetts General Hospital, Harvard Medical School, Boston, MA 02114, USA

[2]Graduate Program in Immunology, Harvard Medical School, Boston, MA 02115, USA

[3]Lead Contact

SUMMARY

Generating robust $CD4^+$ T-helper cell type 1 (Th1) responses is essential for protective vaccine-induced type 1 immunity. Here, we examine whether immunization formulation associated with enhanced vaccine efficacy promotes antigen targeting and cell recruitment into lymph node (LN) niches associated with optimal type 1 responses. Immunization with antigen and Toll-like receptor agonist emulsified in oil leads to an increased differentiation of IFNγ/TNF-α^+ polyfunctional Th1 cells compared to an identical immunization in saline. Oil immunization results in a rapid delivery and persistence of antigen in interfollicular regions (IFRs) of the LN, whereas without oil, antigen is distributed in the medullary region. Following oil immunization, CXCL10-producing inflammatory monocytes accumulate in the IFR, which mobilizes antigen-specific $CD4^+$ T cells into this niche. In this microenvironment, $CD4^+$ T cells are advantageously positioned to encounter arriving IL-12-producing inflammatory dendritic cells (DCs). These data suggest that formulations delivering antigen to the LN IFR create an inflammatory niche that can improve vaccine efficacy.

Graphical Abstract

*Correspondence: aluster@mgh.harvard.edu.

AUTHOR CONTRIBUTIONS

Conceptualization, J.L., C.L.S., and A.D.L.; Methodology, J.L., A.J.O., C.L.S., and A.D.L.; Formal Analysis, J.L. and A.J.O.; Investigation, J.L., A.J.O., C.L.S., and A.D.L.; Resources, A.D.L.; Writing–Original Draft, J.L. and A.D.L.; Writing – Review & Editing, J.L., A.J.O., C.L.S., and A.D.L.; Supervision & Project Administration, A.D.L.; Funding Acquisition, A.D.L.

SUPPLEMENTAL INFORMATION

Supplemental Information can be found online at https://doi.org/10.1016/j.celrep.2020.107679.

DECLARATION OF INTERESTS

The authors declare no competing interests.

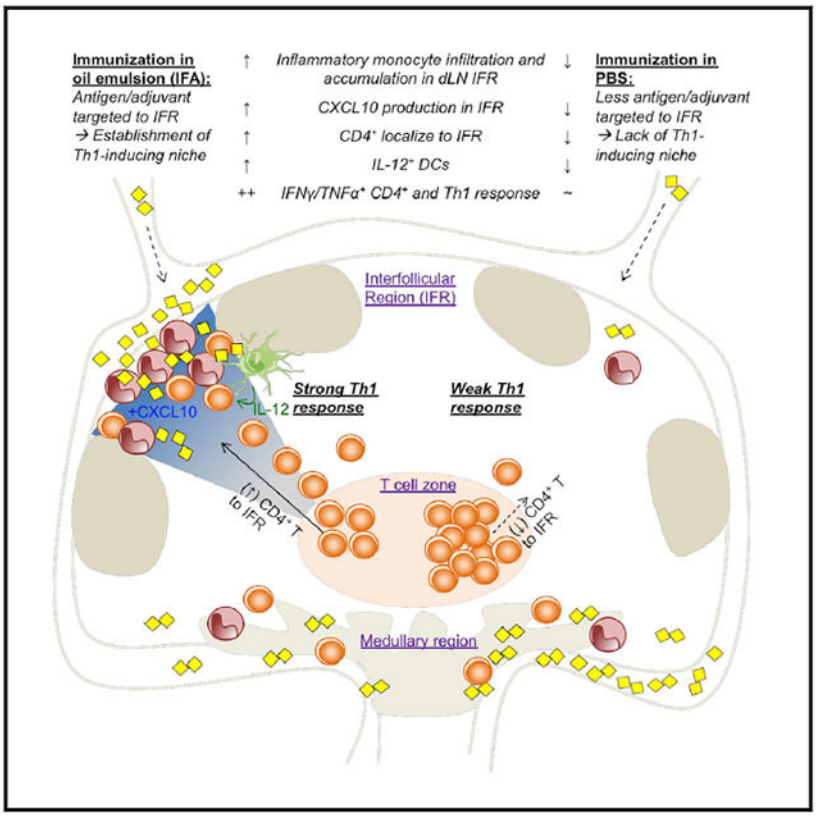

In Brief

Lian et al. demonstrate that emulsification targets antigen/adjuvant to interfollicular regions of the lymph node. Infiltrating inflammatory monocytes localize to this specialized niche, where they produce CXCL10 and attract $CD4^+$ T cells for advantageous positioning to encounter IL-12^+ DCs, leading to the generation of enhanced type 1 immune responses.

INTRODUCTION

The generation of a protective adaptive immune response requires the convergence of multiple cell types in the same anatomical location. Secondary lymphoid organs serve as strategically positioned hubs where circulating naive lymphocytes accumulate to survey antigens and mount adaptive immune responses. After pathogen encounter or immunization at a barrier surface, antigens arrive to the draining lymph node (dLN) via afferent lymphatics primarily through direct drainage or carried by migratory dendritic cells (DCs). Upon antigen recognition in the proper context of costimulatory signals, $CD4^+$ T cells can differentiate into T-helper type 1 (Th1) cells that secrete high levels of interferon-gamma (IFNγ) and tumor necrosis factor alpha (TNF-α) and are critical for immunity against intracellular pathogens and tumor cells (Zhu et al., 2010). $CD4^+$T cell priming and lineage commitment involves multiple interactions between T cells and DCs in the LN and is facilitated by the LN microanatomy (Celli et al., 2005; Itano et al., 2003; Junt et al., 2008; Mempel et al., 2004).

Chemokines are essential cues responsible for directing immune cell positioning at homeostasis and in response to inflammation (Griffith et al., 2014). Chemokine microenvironments support the organization of the LN into distinct compartments. The interfollicular region (IFR) connects the subcapsular sinus (SCS) with the LN cortex and separates the CXCL13-rich B cell follicles in the LN periphery from the CCL19- and CCL21-rich T cell zone in the paracortex. The stromal cell network in the IFR contains channels between B cell follicles that facilitate DC entry from the LN sinus and their accumulation along the cortical ridge between the T and B cell zones. Thus, the IFR is anatomically positioned to serve as a crossroads that bridges innate and adaptive immunity (Katakai et al., 2004a).

The IFR has been shown to play an important role in type 1 inflammation. Previous work from our lab demonstrated that the upregulation of CXCR3 on $CD4^+$ T cells is required for optimal Th1 differentiation and their intranodal positioning to peripheral areas of the LN such as the IFR, where the CXCR3 ligands CXCL9 and CXCL10 are highly upregulated in response to type-1-inducing stimuli (Groom et al., 2012). The IFR has also been shown to play an important role as the site where $CD4^+$ T cells co-localize with cross-presenting DCs and deliver help to $CD8\alpha^+$ cytotoxic lymphocytes (Eickhoff et al., 2015; Hor et al., 2015; Qi et al., 2014), further underscoring the importance of this region in generating a robust immune response to type 1 pathogens.

The induction of polyfunctional Th1 cells is an important element of a protective vaccine response (Darrah et al., 2007), but how vaccine components contribute to the generation of niches capable of supporting optimal Th1 differentiation *in vivo* is not completely understood. Vaccines formulated in oil emulsions have been shown to promote the generation of robust antibody titers and cellular immunity (Coffman et al., 2010; Di Pasquale et al., 2015). Although responses to oil emulsions have been partially attributed to the establishment of an antigen depot at the injection site, studies using alum indicate mechanisms of action independent of the injection site depot (Hutchison et al., 2012; Noe et al., 2010). Injected antigen, depending on the size, can directly access afferent lymphatics and rapidly enter the dLN (Roozendaal et al., 2009; Sixt et al., 2005), and the pattern of antigen dispersal in the LN after immunization can have profound effects on T cell activation (Gerner et al., 2017). Thus, in addition to antigen and adjuvant, formulation is an important component of a vaccine that requires further understanding of its contribution to the LN response to immunization. We used Incomplete Freund's adjuvant (IFA), which consists of non-metabolizable mineral oil and surfactant (paraffin oil and mannide monooleate), to better understand how oil emulsion might affect antigen distribution in the dLN and whether these patterns could lead to differences in the establishment of microenvironments capable of supporting robust Th1 differentiation. We compared immunizations containing the identical combination of the model antigen ovalbumin (OVA) and the Toll-like receptor 4 (TLR4) agonist lipopolysaccharide (LPS) either in saline or emulsified in IFA. Unlike the formulation in saline, IFA-containing immunization accumulated in the dLN IFR, resulting in the coordinated positioning of innate and adaptive immune cells into this specialized niche that enhanced polyfunctional Th1 differentiation and the type 1 immune response.

RESULTS

Immunization with IFA Leads to a More Robust Th1 Response to TLR Ligand

To understand the vaccine components required to induce a robust type 1 immune response, we immunized mice in the footpad with OVA protein as a model antigen, with or without LPS (5 μg per footpad), either in saline or emulsified 1:1 in IFA (Figure 1A). IFA is a well-established research compound known to boost the response to immunization but does not contain bacterial components found in Complete Freund's adjuvant, thereby allowing us to separate the type 1 skewing factor (the TLR4 ligand LPS) from the carrier condition (saline or oil emulsified). Despite the presence of a high dose of TLR agonist, immunization with OVA and LPS in PBS (OVA/LPS) did not result in as robust of a type 1 response as the identical dose of OVA and LPS emulsified in IFA (OVA/LPS/IFA). Significant IFNγ production from dLN cells cultured with OVA was observed only in mice immunized with the combination of OVA/LPS/IFA, but not after immunization with OVA alone, OVA/IFA, or OVA/LPS (Figure 1B). Since OVA/IFA without TLR agonist (LPS) was unable to induce an IFNγ response in the dLN, we proceeded to try to better understand why immunization with the identical concentration of antigen and TLR agonist was not sufficient to induce a high level of IFNγ production without emulsification in IFA.

To determine whether the increased IFNγ recovered from the supernatants of OVA/LPS/IFA-immunized dLNs cultured with OVA was associated with increased $CD4^+$ Th1 cell responses, intracellular cytokine staining of these same OVA-cultured cells was performed. There was an increased frequency of polyfunctional Th1 cells co-producing TNF-α and IFNγ in OVA-cultured dLN cells after OVA/LPS/IFA immunization, compared to OVA or OVA/LPS (Figures 1C and 1D).

Compared to immunization with OVA alone, LN size and cellularity were increased after immunization with OVA/LPS/IFA but not after OVA/LPS (Figures 1E and 1F). In addition, OVA/LPS/ IFA immunization generated the highest levels of OVA-specific IgG1 and IgG2a antibodies in the serum at 21 days post-immunization, compared to OVA alone or OVA/LPS (Figure 1G). OVA/LPS immunization did cause an increase in OVA-specific serum IgG2a compared to OVA alone, demonstrating the importance of TLR agonist (LPS) to provide type 1 skewing signals.

Collectively, these data suggest that while the presence of a high dose of LPS in an immunization can generate some type 1 skewed antibodies, it is not sufficient to lead to enhanced Th1 differentiation. The most robust type 1 antibody production and Th1 differentiation is achieved only when antigen and LPS are emulsified in IFA.

IFA-Containing Immunization Promotes Antigen Targeting to IFRs of the LN

Since immunization with a high dose of LPS did not result in robust type 1 responses unless it was emulsified in IFA, we hypothesized that changes to the nature of the immunization formulation after emulsification may be altering the antigen distribution pattern in the dLN and thereby affecting downstream immune pathways, leading to increased Th1 differentiation. To test this, we labeled OVA with the fluorescent small molecule dye Alexa Fluor 488 (AF488-OVA) and immunized mice with either AF488-OVA/LPS or AF488-

OVA/LPS/IFA and performed light sheet microscopy on CUBIC (clear, unobstructed brain imaging cocktails and computational analysis)-cleared LNs (Abe et al., 2016). This technique allowed us to fully appreciate the distribution of antigen in three dimensions, and particularly better visualized antigen in the cortical areas of the LN in a manner that traditional confocal imaging of frozen sections did not adequately highlight. Light sheet microscopy revealed that OVA/LPS/IFA was distributed to different regions of the dLN compared to OVA/LPS. Twenty-four hours after OVA/LPS/IFA immunization, labeled OVA appeared localized in cortical regions to a greater degree, compared to OVA/LPS immunization, and demonstrated a ringed pattern suggestive of antigen deposition to the IFRs surrounding B cell areas (Figure 2A; Videos S1 and S2). When performed alongside labeling of LN follicles and high endothelial venules (HEVs), we confirmed that the pattern of antigen distribution in the IFR after OVA/LPS/IFA was established as quickly as 6 h following immunization, persisting through 24 h and 72 h post-immunization (Figure 2B; Videos S3, S4, S5, S6, S7, and S8). The kinetics suggest that this effect was due to passive drainage of the antigen from the tissue to the dLN, potentially promoting early activation of this LN niche preceding tissue-derived dendritic cell migration. AF488-OVA/LPS/ IFA immunization resulted in a slightly dimmer signal in dLNs, likely due to the emulsification process that generates a slightly opaque white solution.

In order to determine the overall magnitude of antigen taken up by cells in the dLN, we analyzed the dLNs after each immunization containing fluorescently labeled OVA by flow cytometry at various time points. Injected OVA rapidly entered the dLN and could be detected as early as 1 h after immunization, and there was a similar number of OVA^+ cells in the dLNs following AF488-OVA/LPS or AF488-OVA/LPS/IFA immunization at each time point analyzed (Figures S1A and S1B). These data confirm that passively draining antigen can rapidly reach the dLN after immunization with either combination and suggest that the effect of IFA is not simply the result of an overall increase in the number of cells in the dLN that can acquire antigen, but is due to the persistence of antigen in different locations within the LN.

Inflammatory Monocytes Infiltrate the LN from the Blood in Response to IFA-Containing TLR Immunization

Although we did not observe a difference in the total number of OVA^+ cells in the dLN between the immunizations, we hypothesized that the change in antigen distribution seen after emulsification may have altered which specific subsets of cells were acquiring antigen after immunization. To identify which mononuclear phagocyte ($SSC^{hi}Lin^-CD11b^+$ or $CD11c^+$) subsets in the dLN had acquired antigen and might be responsible for augmenting the immune response after OVA/LPS/IFA, we performed additional flow cytometry analysis of dLNs immunized with AF488-OVA/LPS or AF488-OVA/LPS/IFA at various time points using the gating strategy shown in Figure S2. We found that compared to OVA/LPS, OVA/LPS/IFA immunization caused an increased accumulation of OVA^+ inflammatory monocytes at the earlier time points of 6 h and 24 h post-immunization, with a trend toward an increase at the later time points of 48–72 h postimmunization (Figure 3A, left panel). The number of OVA^+ $CD8\alpha^+$ DC1s was not different between the two immunizations at any of the time points analyzed (Figure 3A, middle panel). However, when we looked for $CD11c^+$

DCs that expressed MHCII and CD209a/DCSIGN (DCSIGN DCs)—the mouse ortholog for human DC-SIGN (Park et al., 2001), a C-type lectin expressed on $CD11b^+$ DCs associated with TLR4 stimulation and Th1 cell responses (Bergman et al., 2004; Geijtenbeek et al., 2003; Steeghs et al., 2006)—we noticed an increase in the number of OVA^+ DCSIGN DCs at 48 h post-OVA/LPS/IFA immunization with a trend toward an increase at 72 h (Figure 3A, right panel). Total cell numbers of these same populations followed a similar pattern, with an increase in the total number of inflammatory monocytes at 6 h and 24 h after OVA/LPS/IFA immunization compared to OVA/LPS, similar numbers of $CD8\alpha^+$ DCs, and increased numbers of DCSIGN DCs at 48 and 72 h post-immunization (Figure 3B). We did notice an increased population of OVA^+ cells that were SSC^{lo} after OVA/LPS immunization compared to OVA/LPS/IFA immunization (Figure S1), which were also positive for lineage markers (Thy1.2/NK1.1/CD19) and could represent medullary B cells based on the pattern of antigen distribution seen in Figure 2.

To better understand the individual contributions of LPS and IFA to the innate immune response in the dLN to immunization, we further analyzed the early dLN response to various combinations of vaccine components, including OVA/IFA without LPS. OVA/IFA did not induce comparable numbers of either inflammatory monocytes or $CD8\alpha^+$ DCs compared to OVA/LPS/IFA (Figure S3A). Although the high level of inflammatory monocyte accumulation in the dLN was only observed after OVA/LPS/IFA immunization, OVA/LPS induced a similar number of $CD8\alpha^+$ DCs compared to OVA/LPS/IFA. The early increase in $CCR2^+$ inflammatory monocyte accumulation in response to OVA/LPS/IFA was associated with a rapid and robust induction of CCL2 (Figure S3B). OVA/LPS also induced some CCL2 production; however, OVA/IFA without TLR agonist LPS was not able to induce a comparable CCL2 response in the dLN. The levels of the other murine CCR2 ligands, CCL7 and CCL12, were not different between the immunization groups. Taken together, these data suggest that IFA by itself (without LPS) is not the primary driver of the cellular response in this model and that activation of the dLN in response to TLR agonist delivered in an emulsion (OVA/LPS/IFA) induces a robust CCL2 response, resulting in the rapid recruitment of inflammatory monocytes in response to immunization.

Given the rapid increase in both total and OVA^+ inflammatory monocytes in the dLN after OVA/LPS/IFA immunization, we wanted to determine if the early infiltrating inflammatory monocytes were localizing toward areas in the dLN where antigen was deposited following immunization. Although tools to exclusively identify inflammatory monocytes *in situ* are lacking, we took advantage of the fact that inflammatory monocytes highly express CCR2 and immunized CCR2-reporter mice where red fluorescent protein (RFP) expression is driven by the CCR2 promoter (Saederup et al., 2010). Analysis of frozen sections by confocal microscopy showed localization of CCR2-RFP^+ cells at 6 h post-immunization was in a similar pattern as antigen distribution after either OVA/LPS or OVA/LPS/IFA immunization (Figure 3C). Corresponding with the increased infiltration of inflammatory monocytes, there was a much more robust accumulation of CCR2-RFP^+ cells after IFA-containing immunization in the IFR and medullary region. Additional staining of serial sections with CD169 and SIGNR1 to identify LN macrophages (Gray and Cyster, 2012) revealed that CCR2-RFP^+ cells were accumulating near $SIGNR1^+$ medullary sinus and medullary-sinus-related macrophages that reside in medullary regions and the IFR,

respectively (Figure 3D). Among RFP$^+$ cells in the dLN, 75% were of the inflammatory monocyte phenotype (Ly6C$^+$F480$^+$) after OVA/LPS/IFA, although this proportion was lower in OVA/LPS-immunized dLNs (Figure S3C), corresponding to the recruitment of fewer inflammatory monocytes after immunization.

The kinetics of inflammatory monocyte appearance in the LN (as early as 6 h) suggested that their arrival might precede skin-derived cell migration through afferent lymphatics. To determine if inflammatory monocytes originated from the injected tissue, we immunized Kaede transgenic mice in which cells express a photoconvertible green fluorescence protein that will become red upon exposure to violet light (Tomura et al., 2008). Because of the inability of violet light exposure to penetrate to cells in the footpad, we exposed shaved skin at the tail base prior to immunization with OVA/LPS/IFA and harvested inguinal LNs 24 h later, when some DC migration to the LN had begun to take place. Photoconverted red cells in the dLN were predominantly DCs with a negligible proportion of photoconverted CD11b$^+$ cells, with virtually none of these being inflammatory monocytes (Figure 3E), suggesting that inflammatory monocytes were not migrating from the skin. These data demonstrate that OVA/LPS/IFA promotes rapid inflammatory monocyte infiltration into the reactive LN, likely from the blood, where they localize to antigen-containing LN niches targeted by the immunization.

Infiltrating Inflammatory Monocytes Are a Prominent Source of Early, Type-I-IFN-Dependent CXCL10

Previous studies have established the importance of various LN niches involved in CD4$^+$ T cell activation and have identified CXCR3 as a critical receptor that directs CD4$^+$ T cells to the IFR and medullary regions of the LN for optimal Th1 differentiation (Eickhoff et al., 2015; Gerner et al., 2015; Groom et al., 2012; Horet al., 2015; Woodruff et al., 2014). Having found that inflammatory monocytes rapidly infiltrate the reactive LN in large numbers and localize to areas of antigen targeting, we hypothesized that they may play a role as a highly mobile cell capable of amplifying chemokine gradients in order to direct cell localization in the LN. To identify cellular sources of CXCR3 ligands, we utilized REX3 transgenic CXCL9 and CXCL10 reporter mice, in which CXCL9-producing cells are RFP$^+$ and CXCL10-producing cells are blue fluorescent protein-positive (BFP$^+$) (Groom et al., 2012). Twenty-four hours after OVA/LPS/IFA immunization, flow cytometry analysis revealed that inflammatory monocytes highly expressed CXCL10-BFP in the dLN (Figure 4A). The expression pattern among inflammatory monocytes contrasted with that of CD8α$^+$ DCs (DC1s), which highly expressed CXCL9-RFP. Although some neutrophils and CD8α$^+$ DCs were technically CXCL10-BFP$^+$, the mean fluorescence intensity (MFI) of these cells was negligible compared to inflammatory monocytes, suggesting they are only minor contributors (Figure 4B), while inflammatory monocytes made up approximately 80% of CXCL10-BFP^{hi} cells regardless of immunization type (Figure S4A). Analysis of dLN sections 24 h post-immunization showed that BFP^{hi} CXCL10-producing cells were enriched in the IFR after OVA/LPS/IFA, compared to OVA/LPS (Figure 4C), corresponding to the CCR2-RFP$^+$ cell distribution pattern observed in Figure 3C. To determine the localization pattern specifically of CXCL10$^+$ inflammatory monocytes, bone marrow monocytes were isolated from REX3 mice and adoptively transferred into wild-type (WT) mice prior to

OVA/LPS/IFA immunization. Twenty-four hours post-immunization, CXCL10^{+} monocytes were found in the IFR/ cortical regions of dLNs (Figure S4B), matching the pattern of CXCL10 expression seen in immunized REX3 mice.

To determine whether type I or type II IFNs were regulating CXCR3 ligand production during the early response to OVA/LPS/IFA immunization in the LN, we crossed REX3 mice with *ifnar*$^{-/-}$ (REX3/IFNAR$^{-/-}$) and *ifngr1*$^{-/-}$ (REX3/IFNγR$^{-/-}$) mice, respectively. IFNγR knockout (KO) mice do not show gross defects in immune system development (Huang et al., 1993), while IFNAR KO mice have slightly increased levels of circulating monocytes and neutrophils (Müller et al., 1994). Twenty-four hours post-immunization, we observed a decrease in the CXCL10-BFP and CXCL9-RFP signals in the dLNs of REX3/IFNAR$^{-/-}$ but not REX3/IFNγR$^{-/-}$ mice analyzed by confocal microscopy (Figure 4D). Accordingly, flow cytometry analysis showed a reduction in the frequency of total cells in the dLN that express CXCL10-BFP and the frequency of total cells that express CXCL9-RFP in REX3/IFNAR$^{-/-}$ but not REX3/IFNγR$^{-/-}$ mice, including a reduction in the frequency of inflammatory monocytes expressing CXCL10-BFP and a loss of CXCL10-BFP expression signal within these cells (Figures 4E and 4F).

Together, these results show that as a consequence of its antigen-targeting pattern, OVA/LPS/IFA immunization recruits inflammatory monocytes to the IFR, where they produce CXCL10 and establish an inflammatory niche potentially beneficial for supporting Th1 differentiation; this early CXCR3 ligand production is dependent on type I IFN signaling.

IFA-Containing Immunization Promotes Antigen-Specific CD4^{+} T Cell Localization into the IFR

Since we observed a robust accumulation of CXCL10-producing cells in the IFR in response to OVA/LPS/IFA immunization, we hypothesized that this response might direct CD4^{+} T cells out of the deep LN parenchyma toward niches activated by antigen/adjuvant that contain inflammatory signals that promote Th1 differentiation. In orderto visualize antigen-specific CD4^{+}T cell localization in an immunized mouse, we adoptively transferred 2.5 × 10^{5} naive CD4^{+} T cells from actin-GFP/Thy1.1^{+} OTII mice into WT mice and immunized them 1 day later in the presence of FTY720 to retain T cells in the LN to visualize all activated T cells during the course of the experiment (Figure 5A). The localization of OTII cells within the LN was determined relative to B cell staining (Figure S5A). Since we observed relatively few GFP^{+} cells localized to the most central area of B cell follicles, we chose to combine the IFR and B cell regions for quantitation to simplify the classification of the many GFP^{+} cells positioned on the border of B220 staining. By 72 h after OVA/LPS/IFA immunization, the transferred OTII cells had almost completely mobilized out of the deep paracortex/T cell zone, with the vast majority localizing to the peripheral cortical region containing the IFR and B cell areas (Figures 5B, filled circles, and 5C, right panel). However, in mice immunized with OVA/LPS, more transferred CD4^{+}T cells remained in the T cell zone (Figures 5B, open circles, and 5C, middle panel), with a similar proportion of cells in the IFR/B cell areas compared to mice immunized with OVA alone (Figures 5B, open squares, and 5C, left panel). CD4^{+} T cell localization to the medullary region was not

significantly different between the immunization groups. These data demonstrate that immunization with antigen and type-1-skewing agonist alone is not as effective in directing optimal $CD4^+$ T cell positioning in the dLN as the identical mixture emulsified in oil, as OVA/LPS/IFA was able to effectively direct $CD4^+$ T cell mobilization out of the central T cell zone and into the IFR/B cell areas.

To test whether the promotion of $CD4^+$ T cell positioning to IFR/B cell areas after emulsified LPS immunization was unique to IFA or if this effect could be induced by other oil compounds, we examined the antigen-specific $CD4^+$ T cell localization pattern after immunization emulsified in AddaVax (AVx), the research-grade equivalent of the clinically approved squalene oil-based MF59 adjuvant (O'Hagan et al., 2013). Compared to immunization with OVA or OVA/LPS, OVA/LPS/AVx immunization resulted in an increased proportion of $CD4^+$ T cells positioned in the IFR/B cell areas and fewer in the T cell zone, with a similar proportion in the medullary region (Figure S5B). These data suggest that the induction of optimal intranodal $CD4^+$ T cells positioning is not a unique response to IFA-containing immunization but may be one mechanism of enhanced clinical responses to vaccines containing oil emulsions.

In order to test whether the T cell localization pattern we observed required an antigen depot effect at the injection site following immunization with IFA, we performed the same adoptive transfer of naive $CD4^+$ T cells and instead immunized the ear, which allowed us to resect the injection site shortly after immunization (Figure 5D). Ear immunization with OVA/LPS/IFA resulted in $CD4^+$ T cell localization patterns in the LN similar to footpad immunization, with a greater proportion of transferred cells mobilizing out of the T cell zone and moving into the IFR/B cell areas (Figure 5E, filled circles) compared to immunization with OVA alone in PBS (Figure 5E, open squares). Ear resection 1 h after OVA/LPS/IFA immunization did not alter T cell localization patterns (Figure 5E, filled triangles). These data do not rule out any effect of the antigen depot on immunization strength; however, they do suggest that the mechanisms leading to T cell mobilization to the IFR/B cell areas after OVA/LPS/IFA are not strictly dependent on the antigen depot at the injection site and are capable of being initiated by activation resulting from the direct drainage of emulsified antigen and adjuvant to the LN.

IFA-Containing Immunization Generates Enhanced Antigen-Specific Th1 Differentiation That Is Dependent on Monocyte-Derived Cells

In orderto determine the degree of Th1 differentiation among antigen-specific $CD4^+$ T cells, we performed *ex vivo* intracellular cytokine staining in our adoptive transfer model. At 90 h following OVA/LPS/IFA immunization, there was an increase in the total number of transferred OTII $CD4^+$ T cells in the draining LN, as well as increases in the frequency and number of polyfunctional OTII Th1 cells that were able to simultaneously produce IFNγ and TNF-α (Figures 6A–6C). This enhanced differentiation of polyfunctional Th1 cells after OVA/LPS/IFA was similar to our observations without adoptive transfer in OVA cultured LNs (Figure 1C). There was also an increase in the number of inflammatory monocytes and DCSIGN DCs compared to OVA or OVA/LPS, but no difference in the number of $CD8\alpha^+$ DC1s (Figure 6D), similar to our observations without adoptive transfer (Figure 3B).

Approximately two-thirds of the DCs post-OVA/LPS/ IFA immunization were DCSIGN/ MHCII^{+} (Figure 6E), suggesting that this DC subset was potentially contributing to the enhanced generation of Th1 cells in response to OVA/LPS/IFA.

In order to determine if monocyte-derived cells were mediating the effects seen after OVA/LPS/IFA immunization, we analyzed CD4^{+} T cell localization and Th1 differentiation in monocyte/macrophage (MM)-DTR mice *Lysm*^{Cre} *x Csf1r*$^{LsL\text{-}DTR}$) in which administration of diphtheria toxin (DT) depletes cells of the monocyte-macrophage lineage based on dual expression of *lysm* and *csf1r* (Schreiber et al., 2013). We adoptively transferred naive GFP^{+} OTII CD4^{+} T cells into WT or MM-DTR mice and then immunized them with OVA/LPS/IFA in the presence of FTY720 as before. DT was administered to all mice 1 day prior to, immediately after, and 2 days following immunization to maintain the depletion in MM-DTR mice throughout the experiment (Figure 6F). Compared to WT mice, DT treatment resulted in more transferred CD4^{+} T cells remaining in the T cell zone of MM-DTR mice, with fewer cells mobilizing to the IFR/B cell areas of the dLN (Figures 6G and S6A). This corresponded with a decrease in the frequency of inflammatory monocytes and DCSIGN DCs recovered from dLNs of MM-DTR, compared to WT mice (Figure 6H). In MM-DTR mice, DT treatment resulted in reduced Th1 differentiation in response to OVA/LPS/IFA immunization and a trend toward a decrease in the total number of transferred CD4^{+} T cells recovered from the dLN (Figures 6I and 6J).

In order to complement the depletion of monocytes in MM-DTR mice with an approach that does not also target macrophages or rely on DT, we treated WT mice with anti-Gr1 to maintain the depletion of inflammatory monocytes and neutrophils, and we performed the same adoptive transfer of naive GFP^{+} OTII CD4^{+} T cells followed by OVA/LPS/IFA immunization. Compared to isotype control-treated mice, WT mice treated with anti-Gr1 had a reduced proportion of transferred CD4^{+} T cells localized in the IFR/B cell region of the dLN following immunization with OVA/LPA/IFA (Figures S6B and S6C). Taken together, these data suggest that the depletion of monocyte-derived cells impairs optimal CD4^{+} T cell localization in the dLN and the enhanced Th1 differentiation promoted by OVA/ LPS/IFA immunization.

OVA/LPS/IFA Promotes IL-12p40 Production by DCSIGN DCs and Is Produced alongside CXCR3 Ligands in the IFR

Having observed an increased accumulation of DCSIGN DCs in the LN at later time points following OVA/LPS/IFA immunization, we investigated the role for these cells in promoting Th1 differentiation. IL-12 is a pro-inflammatory cytokine that can promote and sustain Th1 differentiation (Ho and Glimcher, 2002; Murphy and Reiner, 2002). In order to determine the key IL-12-producing immune cell population after OVA/LPS/IFA immunization, we performed flow cytometry on immunized IL-12p40-yellow fluorescent protein (IL12-YFP) mice (Reinhardt et al., 2006). Seventy-two hours after OVA/LPS/IFA immunization, we found an increased frequency of IL12-YFP^{+} DCs in the dLN compared to OVA/LPS and OVA immunizations (Figure 7A, upper panels). The frequency of IL12-YFP^{+} DCSIGN DCs was also increased after OVA/LPS/IFA immunization compared to OVA/LPS and OVA immunizations, becoming approximately half of all IL12-YFP^{+} DCs after OVA/ LPS/I FA

immunization (Figure 7A, lower panels). IL12-YFP expression among $CD11b^+$ cells, including neutrophils and monocytes, was not detected (data not shown). IL-12 was critical forTh1 differentiation after OVA/LPS/IFA, as mice that were deficient for IL12b were impaired in their ability to generate increased levels of IFNγ and Th1 differentiation in response to OVA/LPS/IFA, compared to WT (Figure 7B). In order to determine whether IL-$12p40^+$ cells localized to the same areas in the dLN as CXCR3-ligand-producing cells, we crossed IL12-YFP with REX3 mice. Confocal microscopy revealed substantial IL12p40-YFP^+ cell localization alongside CXCR3-ligand-producing cells in the IFR at 72 h after OVA/LPS/IFA immunization (Figure 7C). Although we observed CXCL10-producing cells in other areas of the dLN, such as medullary regions, there were fewer $IL12p40^+$ cells in these regions, suggesting that LN IFRs are unique niches where $CD4^+$ T cells can respond to CXCR3 ligands and also encounter type 1 skewing cytokine signals from $IL12p40^+$ cells that support robust Th1 differentiation. The appearance of $CD8\alpha^+$ DCs and DCSIGN DCs in the LN depended on CCR7, while inflammatory monocytes did not (Figure 7D), suggesting that DCSIGN DCs and inflammatory monocytes may rely on different mechanisms for their migration into the reactive LN. Together, these data demonstrate that early-infiltrating, $CXCL10^{hi}$, CCR7-independent inflammatory monocytes cooperate with later-arriving, CCR7-dependent, IL-12^+ DCSIGN DCs to create a niche in the dLN IFR that promotes optimal Th1 differentiation.

DISCUSSION

In this study, we found that immunization in oil formulation was superior to saline in promoting antigen targeting in the LN IFR and enhancing Th1 responses to TLR agonist in the dLN. This unique pattern of antigen deposition within the LN correlated with a rapid and enhanced recruitment of circulating inflammatory monocytes into the dLN and accumulation in the IFR. Inflammatory monocytes highly upregulated CXCL10 in a type-I-IFN-dependent manner, and this early LN response amplified CXCR3 ligand gradients to direct $CD4^+$ T cell localization toward the IFR. $CD4^+$ T cell localization to these niches was important for encountering $DCSIGN^+$ IL-12-producing DCs for robust differentiation into polyfunctional Th1 cells. These findings demonstrate that the formulation of an immunogen can have a significant effect on antigen localization and directing immune cell positioning within the LN and can be utilized for the development of more effective vaccines.

Previous work has established CXCR3 and its ligands CXCL9 and CXCL10 (CXCL11 is functionally absent in C57BL/6 mice) as a critical chemokine system that directs intranodal positioning of $CD4^+$ T cells to the IFR for optimal Th1 differentiation (Groom et al., 2012). Using the REX3 reporter mouse developed in that study, we identified Ly6C/$CCR2^+$ inflammatory monocytes as comprising the majority of $CXCL10^{hi}$-expressing cells. IFA-containing immunization promoted the accumulation of $CCR2^+$ cells in the proximity of SIGNR1 $^+$ macrophages in LN IFRs and the up-regulation of CXCL10-producing inflammatory monocytes in LN IFRs. Early CXCR3 ligand production was dependent on the ability to sense type I IFNs, which agrees with previous studies showing that blocking type I IFN signaling impairs early CXCL10 in the LN IFR during the primary antiviral response, and LN macrophages are important contributors to early type I IFN production in this niche (Chatziandreou et al., 2017; Sung et al., 2012). Our data suggest that by targeting

immunization to the LN IFR, OVA/LPS/IFA immunization supports $CD4^+$ T cell recruitment to these areas through the rapid recruitment of inflammatory monocytes that can respond to type I IFNs and produce CXCL10 in these regions. However, further translational studies are needed to determine whether these kinetics and activation patterns can be similarly induced via different routes of administration.

We observed that CXCL9-RFP^{hi}-producing cells were mainly restricted to DC1. Indeed, CXCL9 has been shown to act in the prepositioning of memory $CD8^+$ T cells for activation during the recall response, and its production is more reliant on type II IFN and sustained by T-cell-derived IFNγ later in the immune response (Groom and Luster, 2011; Kastenmüller et al., 2013; Sung et al., 2012). These findings suggest that CXCL9-expressing DCs might play an important role in $CD8^+$ T cell activation, whereas $CD4^+$ T cells could potentially be more dependent on CXCL10 from monocyte-derived cells and $CD11b^+$ DCs, although this may depend on the nature of the inflammatory stimulus. However, whether any bias exists toward CXCL9 or CXCL10 between $CXCR3^+$ $CD8^+$ and $CD4^+$ T cells, and whether these requirements change during different phases of acute inflammation and memory recall, requires further study.

Together, these results suggest that $SIGNR1^+$ LN macrophages might be potential upstream mediators of Inflammatory monocyte activation targeted by OVA/LPS/IFA. We did not observe CXCR3 expression on Inflammatory monocytes (data not shown), but whether LN macrophages play a role In Intranodal recruitment and activation of Inflammatory monocytes through the release of other chemoattractants needs further study and will depend on the development of better tools to Interrogate these populations. Because of a high degree of overlap In the expression of genes and cell-surface molecules during inflammation, exclusively depleting monocytes, and not other DCs and/or myeloid cell populations, remains difficult. It Is also possible that oil emulsions may target additional populations of LN-resident Immune (Bajenoff et al., 2006a; Gaya et al., 2018; Gerneret al., 2015; Kastenmüller et al., 2012) and/or stromal (Bajenoff et al., 2006b; Katakai et al., 2004b; Rodda et al., 2018) cells positioned within the IFR that could contribute to early Innate activation of this niche. In addition, DC1s In the IFR of the LN serve as cross-presenting DCs and platforms for the delivery of $CD4^+$ help to cytotoxic T lymphocytes (CTLs) (Eickhoff et al., 2015; Hor et al., 2015). Our finding that immunization In IFA promotes CXCR3 ligand and IL-12 production In IFRs may suggest that efficient delivery of antigen and adjuvant to these regions by using oil formulations could be a way to promote DC1 cross-presentation and CTL responses.

Our finding that $DCSIGN^+$ DCs but not Inflammatory monocyte accumulation In the LN depends on CCR7 suggests that optimal Th1 responses require cooperation between these two cell types. Migration of DCs from the skin to the LN requires CCR7 (Ohl et al., 2004), and their accumulation In the LN can take 24 h after activation (Itano et al., 2003). Accordingly, we did not see the Increased accumulation of $DCSIGN^+$ DCs until 48 h after immunization, while Increased numbers of Inflammatory monocytes could be detected within LNs as early as 6 h post-immunization and agree with prior studies demonstrating rapid monocyte recruitment to the Inflamed LN Independent of CCR7-mediated migration (Nakano et al., 2009; Palframan et al., 2001). During this early activation period, rapidly

mobilized inflammatory monocytes can react to potent, but tightly regulated, inflammatory mediators induced by antigen/adjuvant passively draining the LN, including responses by LN-resident cells, such as macrophage-derived type I IFNs. Inflammatory monocyte activation In the IFR may therefore be beneficial to promote the timely formation of LN niches and amplify chemokine gradients contributing to the prepositioning of $CD4^+$ T cells to these regions, which serve as corridors for DCs arriving from the periphery (Schumann et al., 2010; Ulvmar et al., 2014). In response to OVA/LPS/IFA immunization, we found DCSIGN DCs, but not $CD11b^+$ Inflammatory monocytes, to be a major population of IL-12p40-expressing cells and that this molecule was required for enhanced IFNγ production and Th1 differentiation. Although IL-12p40 Is a subunit for both IL-12 and IL-23, IL-23 helps drive Th17 differentiation and IL-17 production but not IFNγ production (Aggarwal et al., 2003; Langrish et al., 2005); therefore, we believe IL-12 to be the relevant cytokine contributing to enhanced Th1 differentiation in our model. These $IL\text{-}12p40^+$ migratory DCSIGN DCs may contain Important tissue-derived information that the Inflammatory monocytes infiltrating from blood circulation cannot alone provide. Therefore, our data suggest that *in vivo*, an optimal and robust Th1 response depends on timely and spatially orchestrated action of both CXCL10-producing Inflammatory monocytes and IL-12-producing DCSIGN DCs.

Studies utilizing structurally modified TLR agonists and a physical linkage of protein and TLR agonist Into a conjugate vaccine have shown that more efficient delivery and retention of vaccine components In the draining lymph node can elicit Improved T cell responses (Kastenmüller et al., 2011; Liu et al., 2014; Lynn et al., 2015). Oil emulsions are an additional component that can act as a carrier to modulate the vaccine response without requiring modification of the other underlying vaccine elements. Our results with AddaVax suggest that the promotion of $CD4^+$ T cell positioning to Th1-inducing niches may be a shared property among effective oil adjuvants, though a more comprehensive study directly comparing available oil adjuvants is needed. Nevertheless, Improvements to the formulation of oil emulsions have led to a renewed Interest In their clinical application and reopened their potential as a key component of protective vaccines against viruses and cancer (Bergado Baez et al., 2018; Del Giudice et al., 2018). Here, we identify an Important mechanism by which oil emulsion can enhance the immune response that highlights how microenvironments within the LN can shape the immune response. By directing the intranodal targeting of antigen and adjuvant to the specific IFR microenvironment, oil emulsion promotes the co-localization of immune cells within this region and establishes a niche beneficial for generating the most robust polyfunctional Th1 responses. The development of new formulations that can efficiently deliver vaccine components to these regions could provide a substantial benefit to vaccine efficacy, the prevention of infectious diseases, and the treatment of cancer.

STAR★METHODS

RESOURCE AVAILABILITY

Lead Contact—Further information and requests for resources and reagents should be directed to and will be fulfilled by the Lead Contact, Andrew Luster (aluster@mgh.harvard.edu).

Materials Availability—This study did not generate new unique reagents.

Data and Code Availability—This study did not generate/analyze datasets or code.

EXPERIMENTAL MODELS AND SUBJECT DETAILS

C57BL/6 (WT) mice were obtained from Charles River Laboratories. CCR2-RFP, Actin-eGFP, IL12p40-eYFP, *Il12b*$^{-/-}$, *ifngr1*$^{-/-}$, *LysM*^{cre}, *Csf1r*$^{LsL\text{-}DTR}$, *Ccr7*$^{-/-}$, OTII (male-linked) and Thy1.1 mice were obtained from Jackson Laboratories. *Ifnar*$^{-/-}$ mice (Müller et al., 1994), were a gift from Michel Aguet (University of Zurich, Zurich, Switzerland). REX3-Tg mice were generated by our lab as previously described (Groom et al., 2012). Kaede transgenic mice were obtained from Dr. Osami Kanagawa (RIKEN Institute) (Tomura et al., 2008), rederived at Taconic and then bred at Massachusetts General Hospital. *LysM*^{cre} mice were crossed with *Csf1r*$^{LsL\text{-}DTR}$ to generate MM-DTR mice as previously described (Schreiber et al., 2013). All mice were maintained on the C57BL/6 background. REX3-Tg and IL12p40-eYFP mice were bred and maintained in specific pathogen free (SPF) plus *Helicobacter* and Pasteurella Pneumotropica free conditions at the Massachusetts General Hospital all others were bred and maintained under SPF conditions. Male and female mice were used at 6-12 weeks. All procedures were approved and carried out according to the standards and guidelines set forth by the Institutional Animal Care and Use Committee of Massachusetts General Hospital.

METHOD DETAILS

Immunizations, adoptive transfers—Mice were immunized in the footpad with 50 mg ovalbumin (OVA; grade V, Sigma) with or without 5 mg LPS-EK (Invivogen) in 50 mL of PBS or emulsified 1:1 in Incomplete Freund's Adjuvant (Sigma) or AddaVax (Invivogen). For OTII adoptive transfer experiments, naive CD4^{+}T cells were isolated from Actin-GFP/OT2/Thy1.1^{+} mice using magnetic separation (CD4^{+}CD62L^{+}T cell isolation kit; Stemcell). 2.5 × 10^{5} cells per mouse were injected retro-orbitally 1 day priorto immunization. 1mg/kg FTY720 (Cayman Chemicals) was injected intraperitoneally every other day starting immediately after immunization in order to block T cell egress. For ear immunizations, mice were immunized in the ear pinnae in 20 mL total volume and excised 1 hour after immunization. To deplete monocytes 4ng/g of DT (Sigma-Aldrich), 500ug/mouse αGr-1 (RB6-8C5; BioXCell), or500ug/mouse isotype control (mouse IgG2b, κ; BioXCell) was injected intraperitoneally into mice 1 day priorto immunization, immediately following, and on day 2. In some experiments, OVA protein was labeled with AF488 Protein Labeling Kit (ThermoFisher) according to manufacturer's instructions priorto injection. For REX3 monocyte adoptive transfer, monocytes from bone marrow were isolated using magnetic

separation (Mouse monocyte isolation kit; Stemcell) and 1.0×10^6 monocytes per mouse injected retro-orbitally prior to immunization.

LN restimulation—3×10^5 total cells from dLNs were cultured at 37°C in 5% CO_2 for 3 days in 96-well round bottom plates containing 100 μg/mL OVA protein in 200 μL of complete RPMI (10% heat-inactivated fetal calf serum, 2mmol/L Glutamax, 100U/mL penicillin, 100 μg/mL streptomycin, 0.01M HEPES), and supernatants collected and stored at −80°C. To assess polyfunctional T cell responses from cells in OVA cultures, cells were washed and incubated with 20ng/mL phorbol 12-myristate 13-acetate (PMA) + 1 mg/mL ionomycin in the presence of Brefeldin A in complete RPMI at 37°C for 4 hours. To asses antigen-specific *ex vivo* responses in OTII adoptive transfer experiments, dLNs were harvested 4 days after immunization and restimulated with 20 mg/mL OVA peptide (323-339, Invivogen) + 2 mg/mL soluble αCD28 with Brefeldin A in complete RPMI for 4 hr.

Enzyme-linked immunosorbent assay (ELISA)—Supernatants from restimulated LNs were collected and mouse IFNγ measured by ELISA (BioLegend) according to manufacturer's protocols. Briefly, samples were incubated at room temperature in triplicate with antibody-coated plates for 1 hour, detection antibody for 1 hour, followed by streptavidin-horseradish peroxidase for 30 minutes. TMB substrate solution was added and the reaction stopped with 2M sulfuric acid. Samples were read at 450nm with Softmax Pro Software and concentrations determined from a standard curve. For OVA-specific ELISA, mice were immunized on D0 and given an identical booster on D14, and serum was harvested on D21. High-binding assay plates were coated with 10 μg/mL OVA in PBS at 4°C overnight, then blocked with 5% dried milk at room temperature for 2 hours. Serial dilutions of serum in duplicate were incubated at room temperature with OVA-coated plates for 2 hours, followed by Goat anti-mouse IgG1- or IgG2a-human adsorbed-HRP (Southern Biotech) for 1 hour. 1-step Ultra TMB (ThermoFisher) was added and the reaction stopped with 2M sulfuric acid. Samples were read at 450nm with Softmax Pro Software and reported as OD450 at the appropriate dilution (IgG1, 1:1,000,000; IgG2a, 1:1,000).

Light Sheet Microscopy—Mice were immunized with AF488-OVA and LNs were fixed in 4% PFA, dehydrated in 30% sucrose, and cleared in CUBIC as previously described (Abe et al., 2016). Cleared LNs were embedded in agarose and light sheet microscopy was performed using a Lightsheet.Z1 Microscope (Carl Zeiss). In some experiments, αCD21/35 was labeled with AF647 and MECA79 labeled with AF594 (ThermoFisher microscale protein labeling kits). To label LN follicles and HEVs, AF647-αCD21/35 was injected into the footpad 18 hr prior and AF594-MECA79 i.v. 2 min. prior to harvest.

Flow cytometry—LNs were digested with 0.26 units/mL Liberase DH (Sigma) and 0.1mg/mL DNase I (Sigma) in RPMI at 37°C for 20 min, minced, and passed over a 35 μM filter. Ice-cold RPMI containing 10% FBS and 10mM EDTA was added to stop digestion. Cells were washed twice in ice cold PBS, blocked with anti-CD16/32 (TruStain FcX; BioLegend) at 4°C for 10 min in FACS buffer and stained with indicated antibodies at 4°C for 30 min. For intracellular cytokine staining, after surface staining cells were fixed and

permeabilized with intracellular fixation and permeabilization buffer (ThermoFisher) and stained for intracellular cytokines. Cells were washed and resuspended in FACS buffer and acquired on a Fortessa X-20 flow cytometer (BD Biosciences). Viability was determined using eFluor 780 Fixable Viability Dye (ThermoFisher) and cell counts determined using CountBright counting beads (ThermoFisher). Data was analyzed using FlowJo software (FlowJo, LLC).

Confocal microscopy—LNs were fixed in PLP at 4°C for 4 hr, dehydrated in 30% sucrose overnight, embedded in OCT (Tissue-Tek) and frozen on 2-methylbutane over liquid nitrogen. 12-16 μM sections were cut from approximately the center of the LN using a Cryostat at −20°C (Microm HM 505 E, GMI). Sections were rehydrated in PBS at room temperature for 20 minutes, blocked with 5% normal goat serum in 0.1% Tween-20 in PBS for 30 minutes, and stained with indicated antibodies for 1 hour at room temperature in the dark. If necessary, samples were incubated for an additional hour with secondary antibodies. Coverslips were mounted with ProLong Diamond Antifade Mountant (ThermoFisher) and cured overnight at room temperature in the dark. Images were captured with an LSM 780 Confocal Microscope at 20x magnification and tile scans compiled with Zen Black software (Carl Zeiss). LN regions were defined based on B cell staining using IMARIS software (Bitplane) and center point spots within each region were calculated.

Kaede photoconversion—Kaede transgenic mice (Tomura et al., 2008) were anesthetized and skin patches on both sides of the tail base were shaved and remaining hair removed by application of Nairfor 30 s followed by washing with PBS. Shaved skin patches were exposed to violet light (420 nm) for 5 minutes using a Bluewave LED visible light curing unit (Dymax) equipped with a 420 nm bandpass filter (Andover Corp) with the light source at maximum power, 7.5 cm away from the skin. Mice were immunized subcutaneously in the tail base and inguinal lymph nodes harvested for analysis.

Quantitative PCR—Total RNA was collected from homogenized whole popliteal LNs using TRIzol reagent (ThermoFisher) according to manufacturer's protocol, diluted in RNase-free water, and stored at −80°C. cDNA was prepared using reverse transcription, and gene expression quantitated using a Roche Lightcycler96 Real-Time PCR system and SYBR Green Master Mix (Roche). Values were calculated relative to *Gapdh.* Validated primer pairs were selected from the MGH PrimerBank.

Primers and antibodies

Mouse Primers: *Ccl2* Fwd, 5′-TTA AAA ACC TGG ATC GGA ACC AA-3′; *Ccl2* Rev, 5′-GCA TTA GCT TCA GAT TTA CGG GT-3′; *Ccl7* Fwd, 5′-GCT GCT TTC AGC ATC CAA GTG-3′; *Ccl7* Rev, 5′-CCA GGG ACA CCG ACT ACT G-3′; *Ccl12* Fwd, 5′-GCT GGA CCA GAT GCG GTG-3′; *Ccl12* Rev, 5′-CCG GAC GTG AAT CTT CTG-3′; *GAPDH* Fwd, 5′-GGC AAA TTC AAC GGC ACA GT-3′; *GAPDH* Rev, 5′-AGA TGG TGA TGG GCT TCC C-3′.

Mouse antibodies: Antibodies were from BioLegend unless otherwise noted: FITC-Ly6G (1A8, 127606), PerCP/Cy5.5-Ly6G (1A8, 127616), PE-CCR2 (R&D, 475301, FAB5538P),

AF700-CCR2 (R&D, 475301, FAB5538N), PE/Cy7-CD8α (53–6.7, 100722), AF700-CD8α (53–6.7, 100730), BV786-CD8α (BD, 53-6.7, 563332), PE/Cy7-CD90.1 (OX-7, 202518), BV605-CD11c (N418, 117334), BV605-CD4 (GK1.5, 100451), BV421-Ly6C (HK1.4, 128032), PerCP/Cy5.5-Ly6C (HK1.4, 128012), BV421-IFNg (XMG1.2, 505830), BV786-IFNγ (BD, XMG1.2, 563773), eFluor660-DCSIGN/CD209a (ThermoFisher, MMD3, 50-2094-82), APC-TNFα (MP6-XT22, 506308), APC/Cy7-MHCII (M5/114.15.2, 107628), BV711-F4/80 (BM8, 123147), BUV737-CD11b (BD, M1/70, 564443), BUV395 (BD, 53-2.1, 565257), BUV395-NK1.1 (BD, PK136, 564144), BUV395-CD19 (BD, 1D3, 563557), BUV395-CD3 (BD, 145-2C11,563565), eFluor780 Fixable Viability Dye (ThermoFisher, 65-0865-18), Alexa Fluor 488-B220 (RA3-6B2, 103225), Alexa Fluor 647-B220 (RA3-6B2, 103226), Alexa Fluor 647-CD169 (3D6.112,142408), Biotinylated SIGNR1 (R&D, Polyclonal, BAF1836), BV421-Streptavidin (405226), anti-CD21/35 (BD, 7G6, 553817), anti-PNAd (BD, MECA-79, 553863), anti-CD28 (37.51, 102112), Goat anti-mouse IgG1-HRP, human adsorbed (Southern Biotech, 1070-05), Goat anti-mouse IgG2-HRP, human adsorbed (Southern Biotech, 1080-05), anti-mouse Gr1 (BioXCell, RB6-8C5, BE0075), mouse IgG2b isotype control (BioXCell, MPC-11, BE0086).

QUANTIFICATION AND STATISTICAL ANALYSIS

Statistics were calculated using Prism software (GraphPad) using the following tests: unpaired two-tailed t test (Figures 6F–6J, 7D, and S6), ordinary one-way ANOVA with Tukey's (Figures 1,3E, 4, 5, 6A–6E, 7A, and S5B) or Dunnett's multiple comparisons test (Figures S3A and S3B), or ordinary two-way ANOVA with Sidak's multiple comparisons tests (Figures 3A, 3B, 7B, and S1). Data are shown as mean ± SEM; *p ≤ 0.05, ** ≤ 0.01, *** ≤ 0.001, **** ≤ 0.0001.

Supplementary Material

Refer to Web version on PubMed Central for supplementary material.

ACKNOWLEDGMENTS

This work was supported by grants from the National Institutes of Health (CA204028) and the Cancer Research Institute to A.D.L. and the American Association Cancer Research Basic Science Fellowships Program and the Swiss National Science Foundation Early Postdoctoral Mobility Award to A.J.O.

REFERENCES

Abe J, Ozga AJ, Swoger J, Sharpe J, Ripoll J, and Stein JV (2016). Light sheet fluorescence microscopy for in situ cell interaction analysis in mouse lymph nodes. J. Immunol. Methods 431, 1–10. [PubMed: 26844990]

Aggarwal S, Ghilardi N, Xie M-H, de Sauvage FJ, and Gurney AL (2003). Interleukin-23 promotes a distinct CD4 T cell activation state characterized by the production of interleukin-17. J. Biol. Chem 278, 1910–1914. [PubMed: 12417590]

Bajénoff M, Breart B, Huang AYC, Qi H, Cazareth J, Braud VM, Germain RN, and Glaichenhaus N (2006a). Natural killer cell behavior in lymph nodes revealed by static and real-time imaging. J. Exp. Med 203, 619–631. [PubMed: 16505138]

Bajénoff M, Egen JG, Koo LY, Laugier JP, Brau F, Glaichenhaus N, and Germain RN (2006b). Stromal cell networks regulate lymphocyte entry, migration, and territoriality in lymph nodes. Immunity 25, 989–1001. [PubMed: 17112751]

Bergado Báez G, Hernández Fernández DR, Mazorra Herrera Z, and Sanchez Ramirez B (2018). HER1-based vaccine: Simultaneousactivation of humoral and cellular immune response. Semin. Oncol 45, 75–83. [PubMed: 30318087]

Bergman MP, Engering A, Smits HH, van Vliet SJ, van Bodegraven AA, Wirth H-P, Kapsenberg ML, Vandenbroucke-Grauls CMJE, van Kooyk Y, and Appelmelk BJ (2004). Helicobacter pylori modulates the T helper cell 1/T helper cell 2 balance through phase-variable interaction between lipopolysaccharide and DC-SIGN. J. Exp. Med 200, 979–990. [PubMed: 15492123]

Celli S, Garcia Z, and Bousso P (2005). CD4 T cells integrate signals delivered during successive DC encounters in vivo. J. Exp. Med 202, 1271–1278. [PubMed: 16275764]

Chatziandreou N, Farsakoglu Y, Palomino-Segura M, D'Antuono R, Pizzagalli DU, Sallusto F, Lukacs-Kornek V, Uguccioni M, Corti D, Turley SJ, et al. (2017). Macrophage Death following Influenza Vaccination Initiates the Inflammatory Response that Promotes Dendritic Cell Function in the Draining Lymph Node. Cell Rep. 18, 2427–2440. [PubMed: 28273457]

Coffman RL, Sher A, and Seder RA (2010). Vaccine adjuvants: putting innate immunity to work. Immunity 33, 492–503. [PubMed: 21029960]

Darrah PA, Patel DT, De Luca PM, Lindsay RWB, Davey DF, Flynn BJ, Hoff ST, Andersen P, Reed SG, Morris SL, et al. (2007). Multifunctional TH1 cells define a correlate of vaccine-mediated protection against Leishmania major. Nat. Med 13, 843–850. [PubMed: 17558415]

Del Giudice G, Rappuoli R, and Didierlaurent AM (2018). Correlates of adjuvanticity: A review on adjuvants in licensed vaccines. Semin. Immunol 30, 14–21.

Di Pasquale A, Preiss S, Tavares Da Silva F, and Garcon N (2015). Vaccine Adjuvants: from 1920 to 2015 and Beyond. Vaccines (Basel) 3, 320–343. [PubMed: 26343190]

Eickhoff S, Brewitz A, Gerner MY, Klauschen F, Komander K, Hemmi H, Garbi N, Kaisho T, Germain RN, and Kastenmüller W (2015). Robust Anti-viral Immunity Requires Multiple Distinct T Cell-Dendritic Cell Interactions. Cell 162, 1322–1337. [PubMed: 26296422]

Gaya M, Barral P, Burbage M, Aggarwal S, Montaner B, Warren Navia A, Aid M, Tsui C, Maldonado P, Nair U, et al. (2018). Initiation ofAntiviral B Cell Immunity Relies on Innate Signals from Spatially Positioned NKT Cells. Cell 172, 517–533.e20. [PubMed: 29249358]

Geijtenbeek TBH, Van Vliet SJ, Koppel EA, Sanchez-Hernandez M, Vandenbroucke-Grauls CMJE, Appelmelk B, and Van Kooyk Y (2003). Mycobacteria target DC-SIGN to suppress dendritic cell function. J. Exp. Med 107, 7–17.

Gerner MY, Torabi-Parizi P, and Germain RN (2015). Strategically localized dendritic cells promote rapid T cell responses to lymph-borne particulate antigens. Immunity 42, 172–185. [PubMed: 25607462]

Gerner MY, Casey KA, Kastenmüller W, and Germain RN (2017). Dendritic cell and antigen dispersal landscapes regulate T cell immunity. J. Exp. Med 214, 3105–3122. [PubMed: 28847868]

Gray EE, and Cyster JG (2012). Lymph node macrophages. J. Innate Immun 4, 424–436. [PubMed: 22488251]

Griffith JW, Sokol CL, and Luster AD (2014). Chemokines and chemokine receptors: positioning cells for host defense and immunity. Annu. Rev. Immunol 32, 659–702. [PubMed: 24655300]

Groom JR, and Luster AD (2011). CXCR3 ligands: redundant, collaborative and antagonistic functions. Immunol. Cell Biol 89, 207–215. [PubMed: 21221121]

Groom JR, Richmond J, Murooka TT, Sorensen EW, Sung JH, Bankert K, von Andrian UH, Moon JJ, Mempel TR, and Luster AD (2012). CXCR3 chemokine receptor-ligand interactions in the lymph node optimize CD4+ T helper 1 cell differentiation. Immunity 37, 1091–1103. [PubMed: 23123063]

Ho I-C, and Glimcher LH (2002). Transcription: tantalizing times forTcells. Cell 109, S109–S120. [PubMed: 11983157]

Hor JL, Whitney PG, Zaid A, Brooks AG, Heath WR, and Mueller SN (2015). Spatiotemporally Distinct Interactions with Dendritic Cell Subsets Facilitates CD4+ and CD8+ T CellActivation to Localized Viral Infection. Immunity 43, 554–565. [PubMed: 26297566]

Huang S, Hendriks W, Althage A, Hemmi S, Bluethmann H, Kamijo R, Vilcek J, Zinkernagel RM, and Aguet M (1993). Immune response in mice that lack the interferon-gamma receptor. Science 259, 1742–1745. [PubMed: 8456301]

Hutchison S, Benson RA, Gibson VB, Pollock AH, Garside P, and Brewer JM (2012). Antigen depot is not required for alum adjuvanticity. FA-SEBJ. 26, 1272–1279.

Itano AA, McSorley SJ, Reinhardt RL, Ehst BD, Ingulli E, Rudensky AY, and Jenkins MK (2003). Distinct dendritic cell populations sequentially present antigen to CD4 T cells and stimulate different aspects of cell-mediated immunity. Immunity 19, 47–57. [PubMed: 12871638]

Junt T, Scandella E, and Ludewig B (2008). Form follows function: lymphoid tissue microarchitecture in antimicrobial immune defence. Nat. Rev. Immunol 8, 764–775. [PubMed: 18825130]

Kastenmüller K, Wille-Reece U, Lindsay RWB, Trager LR, Darrah PA, Flynn BJ, Becker MR, Udey MC, Clausen BE, Igyarto BZ, et al. (2011). Protective T cell immunity in mice following protein-TLR7/8 agonist-conjugate immunization requires aggregation, type IIFN, and multiple DC subsets. J. Clin. Invest 121, 1782–1796. [PubMed: 21540549]

Kastenmüller W, Torabi-Parizi P, Subramanian N, Lammermann T, and Germain RN (2012). A spatially-organized multicellular innate immune response in lymph nodes limits systemic pathogen spread. Cell 150, 1235–1248. [PubMed: 22980983]

Kastenmüller W, Brandes M, Wang Z, Herz J, Egen JG, and Germain RN (2013). Peripheral prepositioning and local CXCL9 chemokine-mediated guidance orchestrate rapid memory CD8+ T cell responses in the lymph node. Immunity 88, 502–513.

Katakai T, Hara T, Lee J-H, Gonda H, Sugai M, and Shimizu A (2004a). A novel reticular stromal structure in lymph node cortex: an immuno-platform for interactions among dendritic cells, T cells and B cells. Int. Immunol 16, 1133–1142. [PubMed: 15237106]

Katakai T, Hara T, Sugai M, Gonda H, and Shimizu A (2004b). Lymph node fibroblastic reticular cells construct the stromal reticulum via contact with lymphocytes. J. Exp. Med 200, 783–795. [PubMed: 15381731]

Langrish CL, Chen Y, Blumenschein WM, Mattson J, Basham B, Sedgwick JD, McClanahan T, Kastelein RA, and Cua DJ (2005). IL-23 drives a pathogenic T cell population that induces autoimmune inflammation. J. Exp. Med 201, 233–240. [PubMed: 15657292]

Liu H, Moynihan KD, Zheng Y, Szeto GL, Li AV, Huang B,Van Egeren DS, Park C, and Irvine DJ (2014). Structure-based programming of lymphnode targeting in molecular vaccines. Nature 507, 519–522. [PubMed: 24531764]

Lynn GM, Laga R, Darrah PA, Ishizuka AS, Balaci AJ, Dulcey AE, Pechar M, Pola R,Gerner MY, Yamamoto A,et al. (2015). In vivo characterization of the physicochemical properties of polymer-linked TLR agonists that enhance vaccine immunogenicity. Nat. Biotechnol 88, 1201–1210.

Mempel TR, Henrickson SE, and Von Andrian UH (2004). T-cell priming by dendritic cells in lymph nodes occurs in three distinct phases. Nature 427, 154–159. [PubMed: 14712275]

Müller U, Steinhoff U, Reis LF, Hemmi S, Pavlovic J, Zinkernagel RM, and Aguet M (1994). Functional role of type I and type II interferons in antiviral defense. Science 264, 1918–1921. [PubMed: 8009221]

Murphy KM, and Reiner SL (2002). The lineage decisions of helper T cells. Nat. Rev. Immunol 2, 933–944. [PubMed: 12461566]

Nakano H, Lin KL, Yanagita M, Charbonneau C, Cook DN, Kakiuchi T, and Gunn MD (2009). Blood-derived inflammatory dendritic cells in lymph nodes stimulate acute T helper type 1 immune responses. Nat. Immunol 10, 394–402. [PubMed: 19252492]

Noe SM, Green MA, HogenEsch H, and Hem SL (2010). Mechanism of immunopotentiation by aluminum-containing adjuvants elucidated by the relationship between antigen retention at the inoculation site and the immune response. Vaccine 28, 3588–3594. [PubMed: 20211692]

O'Hagan DT, Ott GS, Nest GV, Rappuoli R, and Giudice GD (2013). The history of MF59(®) adjuvant: a phoenix that arose from the ashes. Expert Rev. Vaccines 12, 13–30. [PubMed: 23256736]

Ohl L, Mohaupt M, Czeloth N, Hintzen G, Kiafard Z, Zwirner J, Blankenstein T, Henning G, and Forster R (2004). CCR7 governs skin dendritic cell migration under inflammatory and steady-state conditions. Immunity 21, 279–288. [PubMed: 15308107]

Palframan RT, Jung S, Cheng G, Weninger W, Luo Y, Dorf M, Littman DR, Rollins BJ, Zweerink H, Rot A, and von Andrian UH (2001). Inflammatory chemokine transport and presentation in HEV:

a remote control mechanism for monocyte recruitment to lymph nodes in inflamed tissues. J. Exp. Med 194, 1361–1373. [PubMed: 11696600]

Park CG, Takahara K, Umemoto E, Yashima Y, Matsubara K, Matsuda Y, Clausen BE, Inaba K, and Steinman RM (2001). Five mouse homologues of the human dendritic cell C-type lectin, DC-SIGN. Int. Immunol 18, 1283–1290.

Qi H, Kastenmüller W, and Germain RN (2014). Spatiotemporal basis of innate and adaptive immunity in secondary lymphoid tissue. Annu. Rev. Cell Dev. Biol 80, 141–167.

Reinhardt RL, Hong S, Kang S-J, Wang ZE, and Locksley RM (2006). Visualization of IL-12/23p40 in vivo reveals immunostimulatory dendritic cell migrants that promote Th1 differentiation. J. Immunol 177, 1618–1627. [PubMed: 16849470]

Rodda LB, Lu E, Bennett ML, Sokol CL, Wang X, Luther SA, Barres BA, Luster AD, Ye CJ, and Cyster JG (2018). Single-Cell RNA Sequencing of Lymph Node Stromal Cells Reveals Niche-Associated Heterogeneity. Immunity 48, 1014–1028.e6. [PubMed: 29752062]

Roozendaal R, Mempel TR, Pitcher LA, Gonzalez SF, Verschoor A, Mebius RE, von Andrian UH, and Carroll MC (2009). Conduits mediate transport of low-molecular-weight antigen to lymph node follicles. Immunity 80,264–276.

Saederup N, Cardona AE, Croft K, Mizutani M, Cotleur AC, Tsou C-L, Ransohoff RM, and Charo IF (2010). Selective chemokine receptor usage by central nervous system myeloid cells in CCR2-red fluorescent protein knock-in mice. PLoS ONE 5, e13693. [PubMed: 21060874]

Schreiber HA, Loschko J, Karssemeijer RA, Escolano A, Meredith MM, Mucida D, Guermonprez P, and Nussenzweig MC (2013). Intestinal monocytes and macrophages are required forT cell polarization in response to Citrobacter rodentium. J. Exp. Med 210, 2025–2039. [PubMed: 24043764]

Schumann K, Lammermann T, Bruckner M, Legler DF, Polleux J, Spatz JP, Schuler G, Forster R, Lutz MB, Sorokin L, and Sixt M (2010). Immobilized chemokine fields and soluble chemokine gradients cooperatively shape migration patterns of dendritic cells. Immunity 82, 703–713.

Sixt M, Kanazawa N, Selg M, Samson T, Roos G, Reinhardt DP, Pabst R, Lutz MB, and Sorokin L (2005). The conduit system transports soluble antigens from the afferent lymph to resident dendritic cells in the T cell area of the lymph node. Immunity 22, 19–29. [PubMed: 15664156]

Steeghs L, van Vliet SJ, Uronen-Hansson H, van Mourik A, Engering A, Sanchez-Hernandez M, Klein N, Callard R, van Putten JP, van der Ley P, et al. (2006). Neisseria meningitidis expressing lgtB lipopolysaccharide targets DC-SIGN and modulates dendritic cell function. Cell. Microbiol 8, 316–325. [PubMed: 16441441]

Sung JH, Zhang H, Moseman EA, Alvarez D, Iannacone M, Henrickson SE, de la Torre JC, Groom JR, Luster AD, and von Andrian UH (2012). Chemokine guidance of central memory T cells is critical for antiviral recall responses in lymph nodes. Cell 150, 1249–1263. [PubMed: 22980984]

Tomura M, Yoshida N, Tanaka J, Karasawa S, Miwa Y, Miyawaki A, and Kanagawa O (2008). Monitoring cellular movement in vivo with photoconvertible fluorescence protein “Kaede” transgenic mice. Proc. Natl. Acad. Sci. USA 105, 10871–10876. [PubMed: 18663225]

Ulvmar MH, Werth K, Braun A, Kelay P, Hub E, Eller K, Chan L, Lucas B, Novitzky-Basso I, Nakamura K, et al. (2014). The atypical chemokine receptor CCRL1 shapes functional CCL21 gradients in lymph nodes. Nat. Immunol 15, 623–630. [PubMed: 24813163]

Woodruff MC, Heesters BA, Herndon CN, Groom JR, Thomas PG, Luster AD, Turley SJ, and Carroll MC (2014). Trans-nodal migration of resident dendritic cells into medullary interfollicular regions initiates immunity to influenza vaccine. J. Exp. Med 211, 1611–1621. [PubMed: 25049334]

Zhu J, Yamane H, and Paul WE (2010). Differentiation of effector CD4 T cell populations (*). Annu. Rev. Immunol 28, 445–489. [PubMed: 20192806]

Highlights

- Oil emulsion targets antigen to the interfollicular region (IFR) of the lymph node
- $CXCL10^+$ monocytes accumulate in the IFR and attract antigen-specific $CD4^+$ T cells
- $CD4^+$ T cells in the IFR are advantageously positioned to encounter $IL\text{-}12^+$ DCs
- Inflammatory niche in the IFR promotes $IFN\gamma/TNF\text{-}\alpha^+$ Th1 cells and type 1 immunity

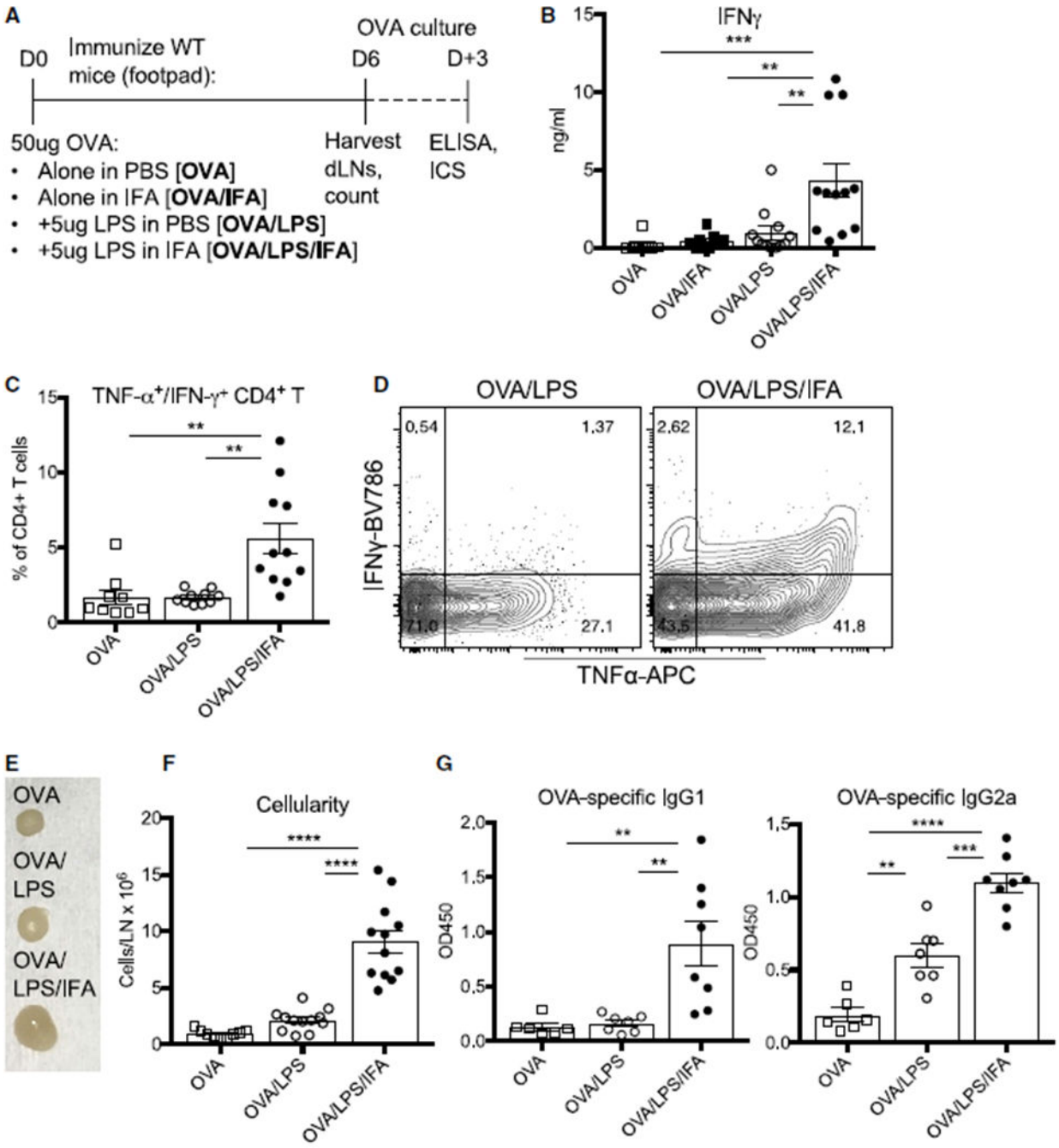

Figure 1. Immunization with IFA Leads to a More Robust Th1 Response to TLR Ligand

(A–F) WT mice were immunized in the footpad with 50 μg OVA with or without 5 μg LPS in PBS or emulsified 1:1 in IFA, and dLNs were harvested 6 days later. (A) Experimental design. (B) dLN cells were cultured with OVA, and IFNγ in the supernatant was measured by ELISA. (C) dLNs cultured with OVA as in (B) were restimulated with phorbol 12-myristate 13-acetate (PMA) and ionomycin and stained for intracellular cytokines. (D) Representative flow cytometry plots of intracellular cytokine staining; gated on live $CD4^+$ T cells. (E) Representative photograph of excised dLNs. (F) Total cellularity of dLNs.

(G) Relative OVA-specific immunoglobulin G (IgG) antibody levels from serum 21 days post-immunization.

In (A)–(F), results are pooled from three independent experiments (n = 9–11 mice per group); in (G), results are pooled from two independent experiments (n = 6–8 mice per group). Data are presented as mean ± SEM; **p ≤ 0.01, ***p ≤ 0.001, ****p ≤ 0.0001.

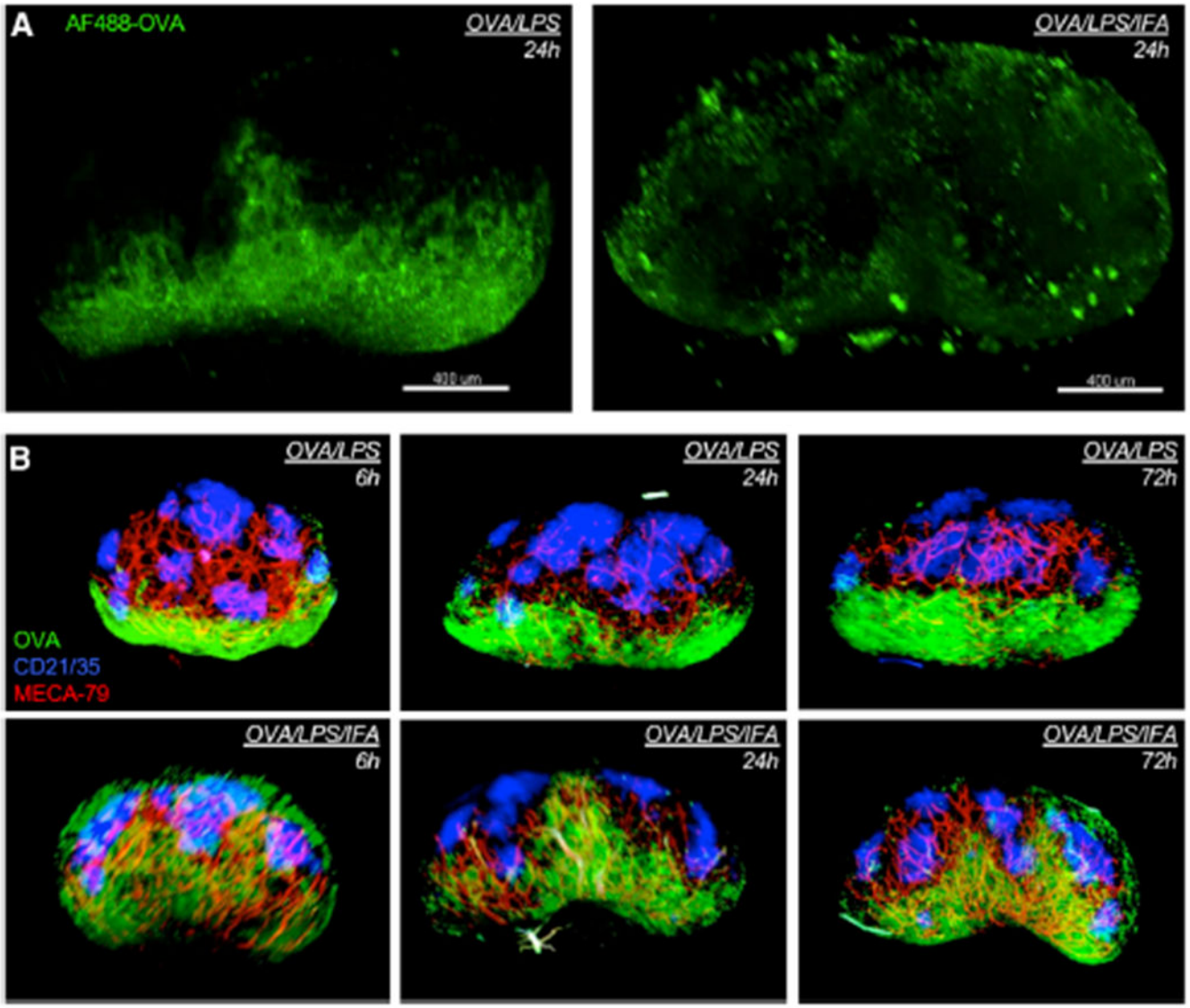

Figure 2. IFA-Containing Immunization Promotes Antigen Targeting to Interfollicular Regions of the LN

(A) WT mice were immunized with AF488-OVA (green) and LPS in PBS (OVA/LPS, left) or AF488-OVA (green) and LPS emulsified in IFA (OVA/LPS/IFA, right). dLNs were harvested after 24 h, cleared in CUBIC, and analyzed by light sheet microscopy. Images are representative still captures from Videos S1 and S2 (n = 3–4 mice per group).

(B) WT mice were immunized as above. *In vivo* labeling with AF647-αCD21/35 (blue; follicles) and AF594-αMECA-79 (red; HEVs) was performed, and dLNs were harvested at the indicated time points. Images are representative still captures from Videos S3, S4, S5, S6, S7, and S8 (n = 2 mice per group).

See also Figure S1.

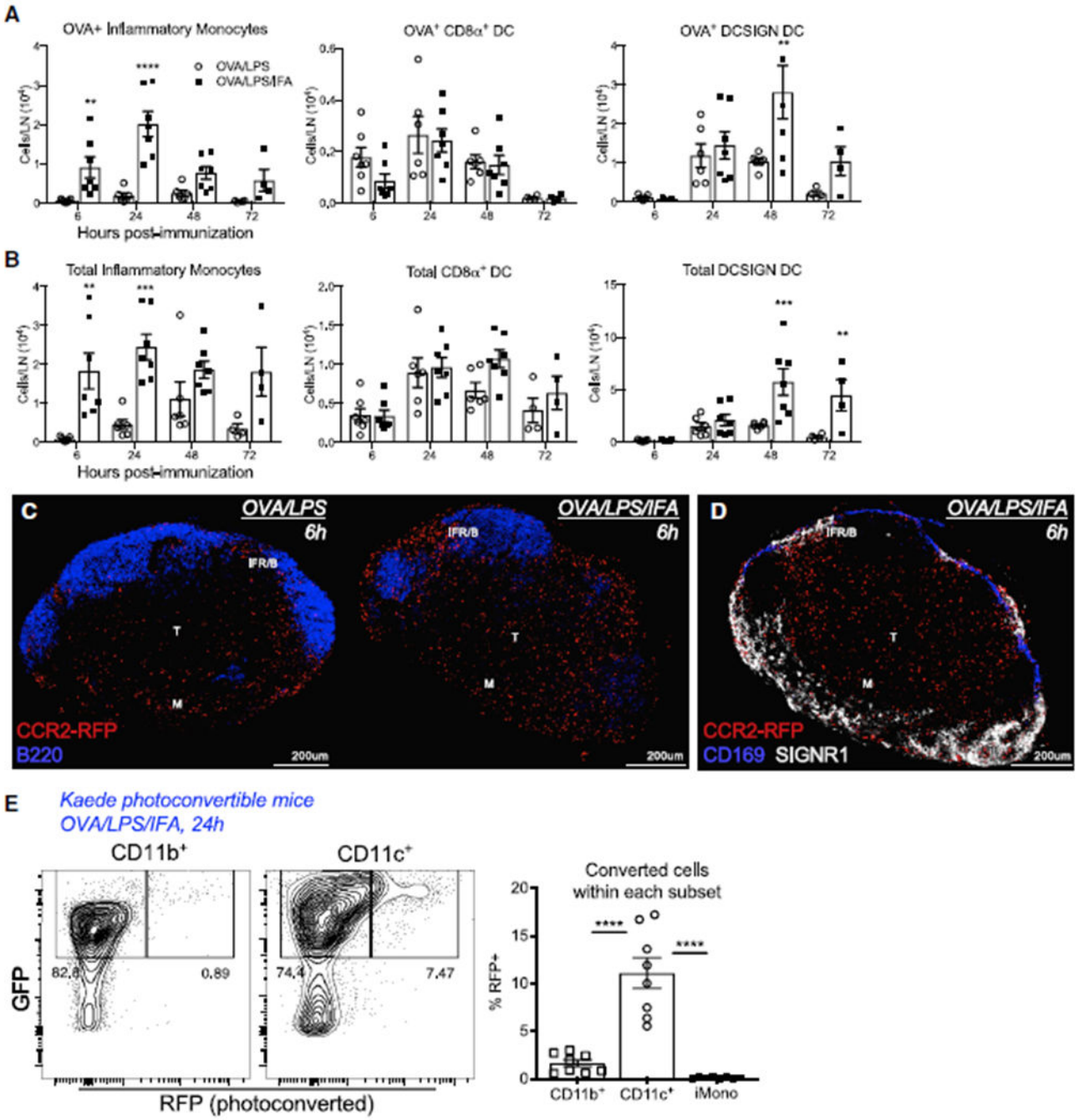

Figure 3. Inflammatory Monocytes Infiltrate the LN from the Blood in Response to IFA-Containing TLR Immunization

(A and B) WT mice were immunized with AF488-OVA/LPS or AF488-OVA/LPS/IFA. dLNs were harvested at the indicated time points and analyzed by flow cytometry according to the gating strategy in Figure S2. (A) AF488-OVA$^+$ cell numbers of the indicated subsets. (B) Total cell numbers of the subsets from (A). Results are pooled from two independent experiments (n = 4–7 mice per group).

(C and D) CCR2-RFP (red) heterozygous reporter mice were immunized as indicated, and dLNs were harvested 6 h later. (C) Frozen sections were stained with B220 (blue) to identify

B cells and analyzed by confocal microscopy. (D) Serial sections from OVA/LPS/IFA immunized dLNs in (C) were stained with CD169 (blue) and SIGNR1 (white) to identify LN macrophages. Images are representative of two independent experiments (n = 5 LNs). (E) Shaved-skin patches at the tail base of Kaede transgenic mice were photoconverted and then immunized with OVA/LPS/IFA, and dLNs (inguinal) were harvested 24 h later. Frequency of photoconverted cells within the indicated subsets was determined by flow cytometry. Results are pooled from three independent experiments (n = 8 mice). Data are presented as mean ± SEM; **p ≤ 0.01, ***p ≤ 0.001, ****p < 0.0001. See also Figure S3.

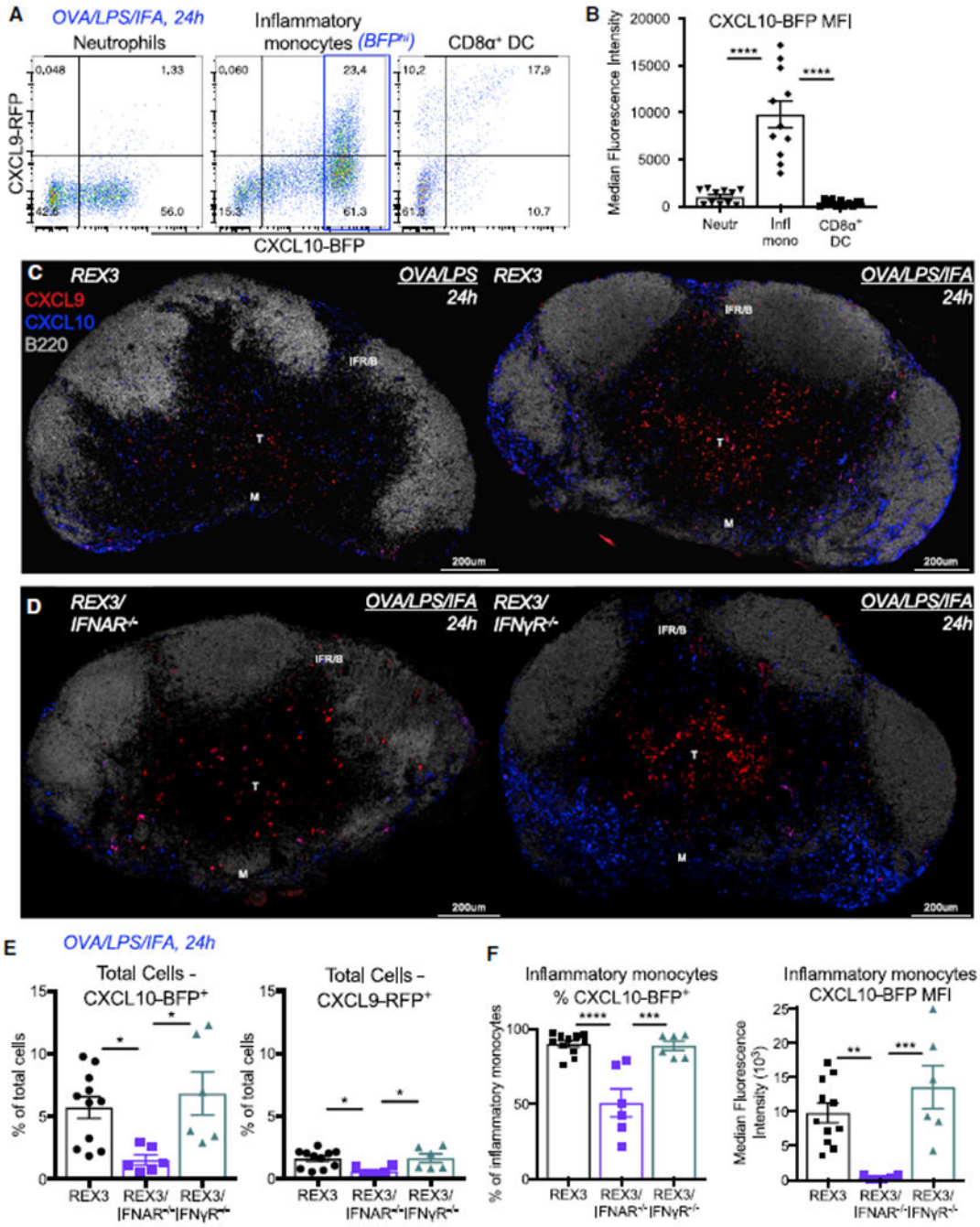

Figure 4. Inflammatory Monocytes Are a Prominent Source of Early, Type-I-Interferon-Dependent CXCL10

(A and B) REX3 reporter mice were immunized with OVA/LPS/IFA, and dLNswere harvested 24 h later for analysis by flow cytometry. (A) Representative plot of CXCL9-RFPand CXCL10-BFP expression with in the indicated cell subsets. (B) Median fluorescence intensity (MFI) of CXCL10-BFP of the indicated cell subsets. Results are pooled from three independent experiments (n = 11 mice).

(C and D) REX3 (C), REX3/IFNAR$^{-/-}$ (D), and REX3/IFNγR$^{-/-}$ mice were immunized as indicated, and dLNs were harvested 24 h later. Frozen sections were stained with B220 and

analyzed by confocal microscopy (B220, gray; CXCL9-RFP, red; CXCL10-BFP, blue). Images are representative of two independent experiments (n = 6 mice per group).
(E and F) dLNs from the indicated strains were harvested 24 h post-OVA/LPS/IFA immunization and analyzed by flow cytometry. (E) Frequency of total cells producing CXCL10-BFP (left) and CXCL9-RFP (right). (F) Frequency of inflammatory monocytes producing CXCL10-BFP (left) and MFI of CXCL10-BFP among inflammatory monocytes (right).
Results are pooled from two or three independent experiments (n = 6–11 per group). Data are presented as mean ± SEM; *p ≤ 0.05, **p ≤ 0.01, ***p ≤ 0.001, ****p ≤ 0.0001. See also Figure S4.

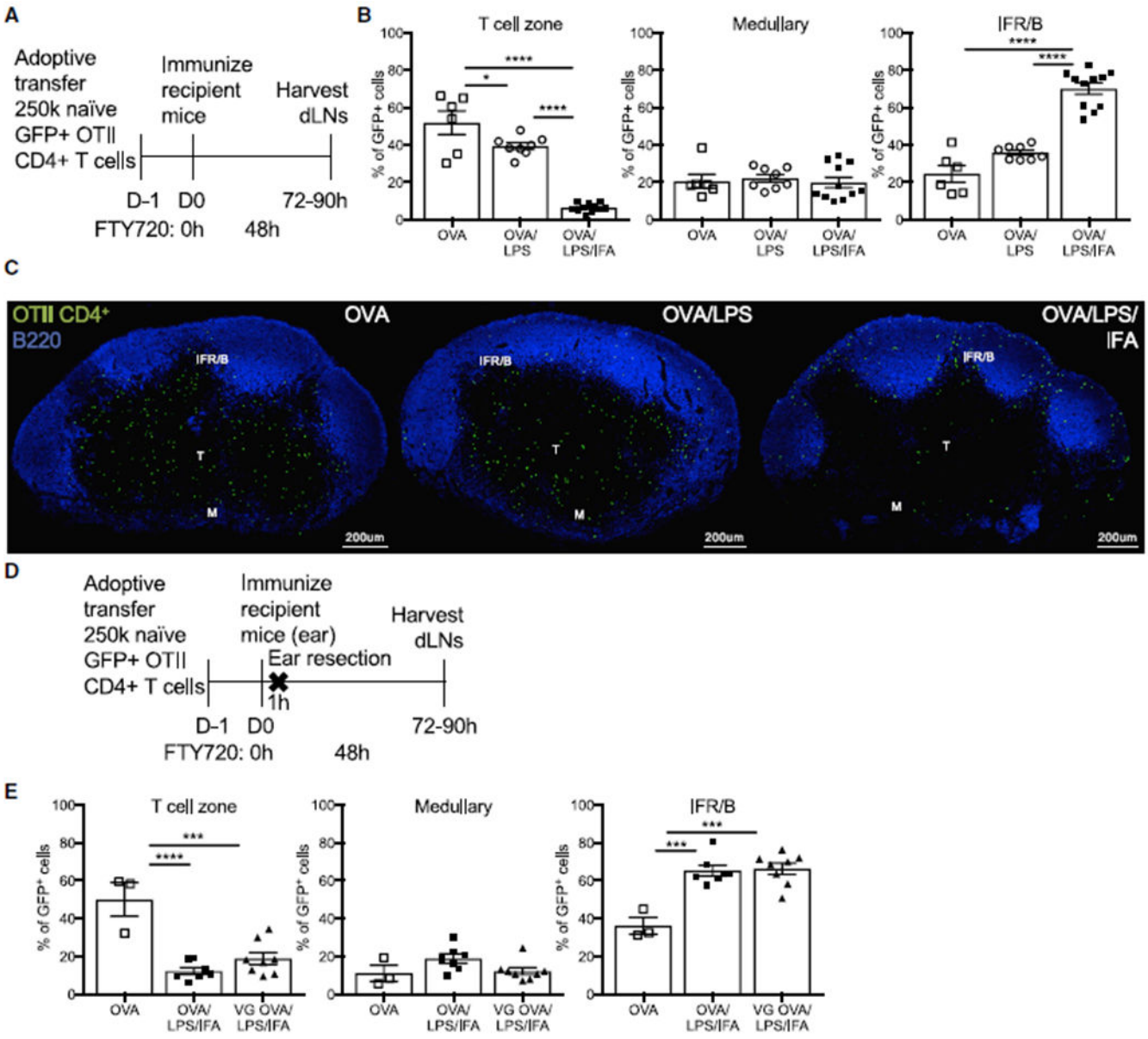

Figure 5. IFA-Containing Immunization Promotes Antigen-Specific CD4$^+$ T Cell Localization into the IFR

Actin-GFP$^+$ naive OTII T cells were adoptively transferred into WT recipients 1 day prior to immunization. FTY720 was administered intraperitoneally (i.p.) at 0 h and 48 h, and LNs were harvested 72–90 h later.

(A) Experimental design.

(B) Transferred CD4$^+$ T cell (green) localization to LN niches, expressed as percentage of GFP$^+$ cells in each LN region from confocal images stained with B220 (blue).

(C) Representative confocal images from (B). Results are pooled from three independent experiments (n = 4–7 mice per group).

(D and E) GFP$^+$ naive OTII cells were transferred as in (A) and recipient mice immunized in the ear in the presence of FTY720, which was excised 1 h after immunization ("VG

OVA/LPS/IFA"). (D) Experimental design. (E) Transferred $CD4^+$ T cell localization at 72–90 h.

Results are pooled from three independent experiments (n = 3–6 mice per group). Data are presented as mean ± SEM; *p ≤ 0.05, ***p ≤ 0.001, ****p ≤ 0.0001. See also Figure S5.

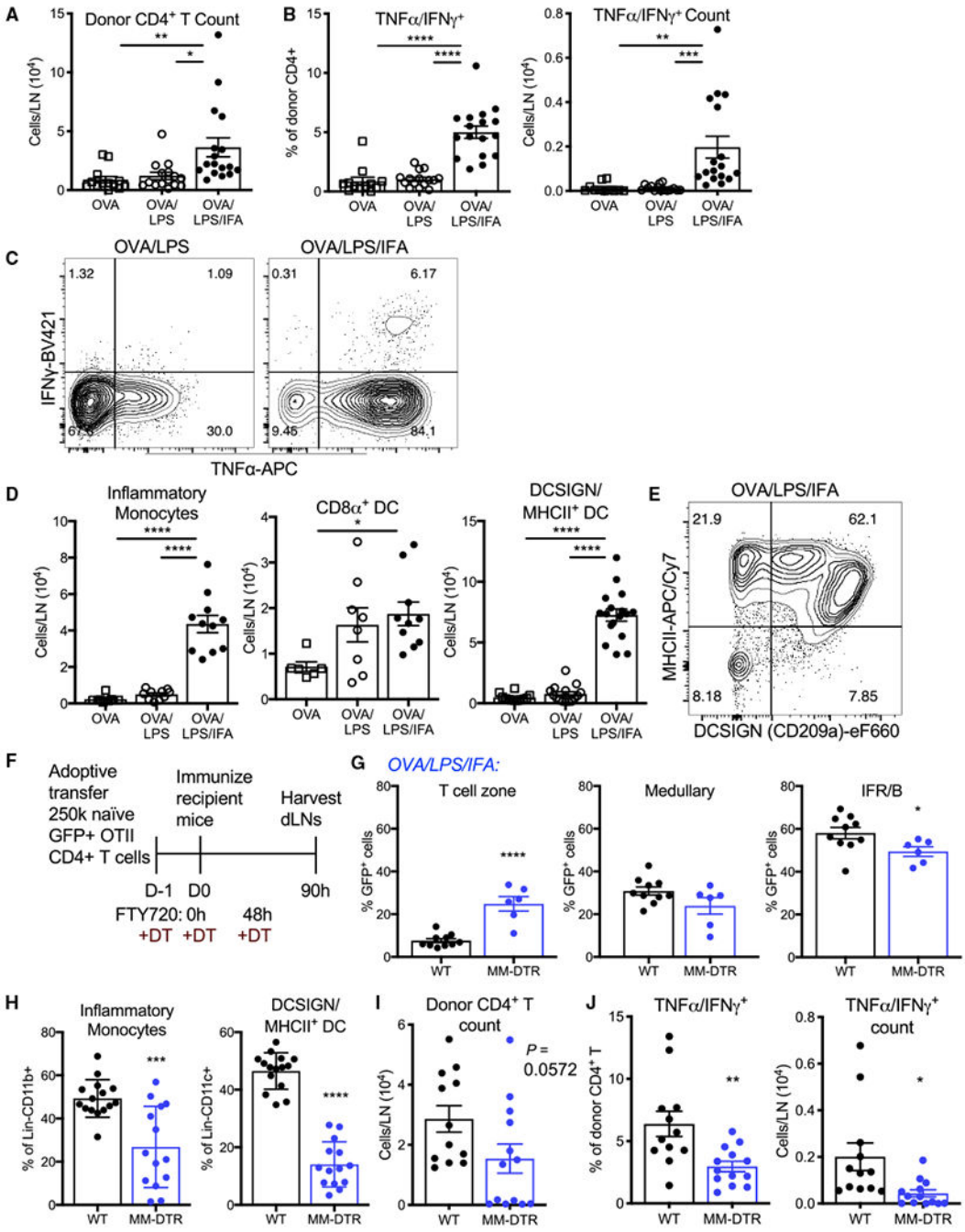

Figure 6. IFA-Containing Immunization Generates Enhanced Antigen-Specific Th1 Differentiation That Is Impaired in the Absence of the Monocyte-Macrophage Lineage

(A-E) GFP$^+$ naive OTII T cells were adoptively transferred into WT recipients 1 day prior to immunization. FTY720 was administered i.p. at 0 h and 48 h, and LNs were harvested at 90 h. (A) Donor CD4$^+$ T cell count. (B) dLN cells were restimulated with OVA peptide (323–339) and αCD28 and stained for intracellular Th1 cytokines. Frequency (left) and number (right) of TNF-α/IFNγ$^+$ cells among donor CD4$^+$ T cells. (C) Representative flow cytometry plots from (B); gated on live donor CD4$^+$ T cells. (D) Cell counts of indicated cell subsets. (E) Representative flow cytometry plot gated on CD11c$^+$ DCs (DCSIGN DCs =

DCSIGN/MHCII^{+}). Results are pooled from four independent experiments (n = 12–17 mice per group).

(F-J) GFP^{+} naive OTII T cells were adoptively transferred into WT or MMDTR recipient mice and immunized with OVA/LPS/IFA. Recipient mice were treated with FTY720 and diphtheria toxin (DT) at the indicated time points, and dLNs were harvested 90 h post-immunization. (F) Experimental design. (G) Transferred CD4^{+} T cell localization to LN niches. Results are pooled from four independent experiments (n = 6–10 mice per group). (H) Frequency of inflammatory monocytes among Lin^{-}CD11b^{+} cells (left) and DCSIGN DCs among Lin^{-}CD11c^{+} cells (right). Results are pooled from five independent experiments (n = 13–14 mice per group). (I) Donor CD4^{+} T cell count. (J) dLN cells were restimulated for 4 h with OVA peptide (323–339) and αCD28 and stained for intracellular Th1 cytokines. Frequency (left) and number (right) of TNF-α/IFNγ^{+} cells among donor OTII CD4^{+}Tcells. Results are pooled from four independent experiments (n = 7–12 mice per group).

Data are presented as mean ± SEM; *p ≤ 0.05, **p ≤ 0.01, ***p ≤ 0.001, ****p ≤ 0.0001. See also Figure S6.

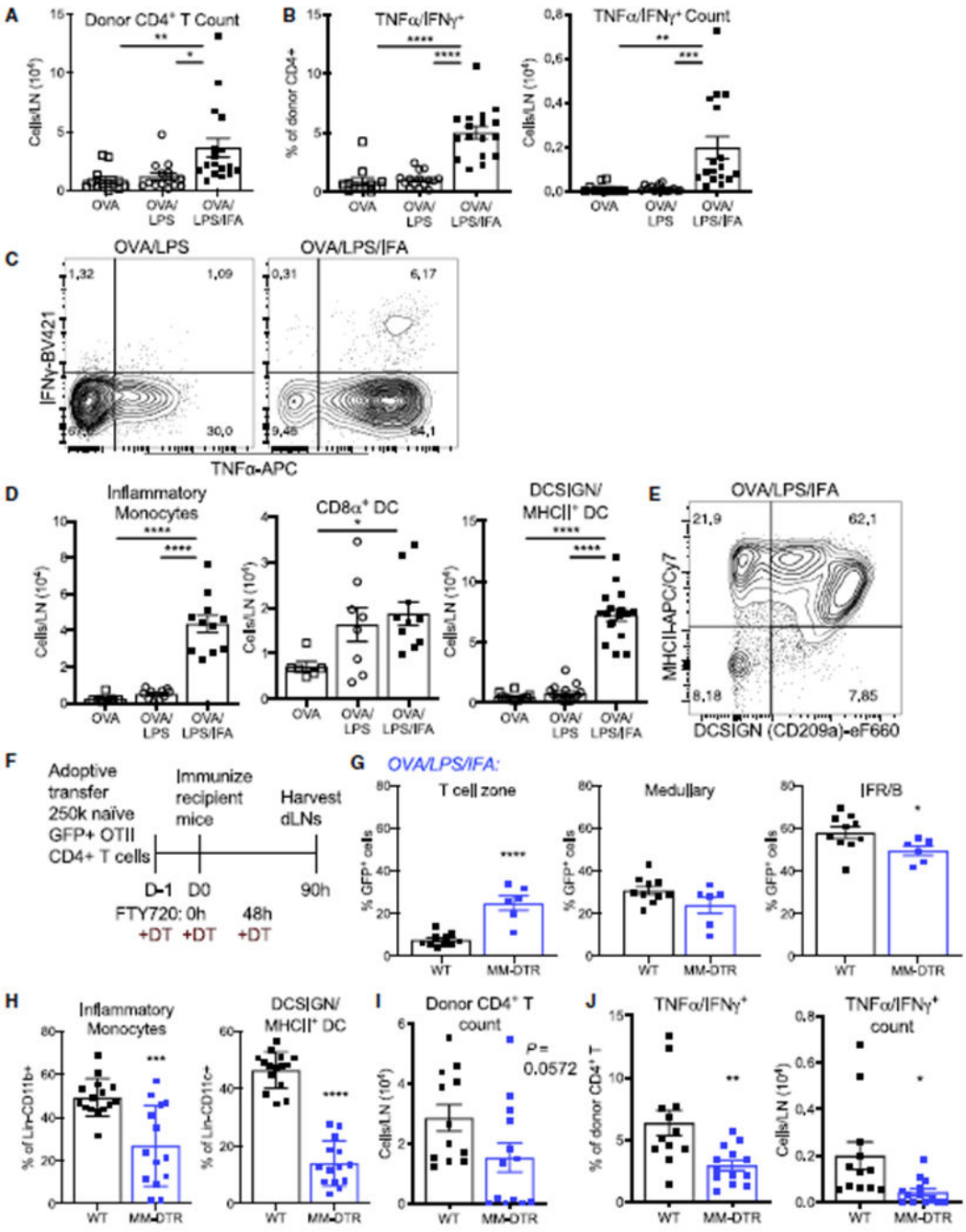

Figure 7. OVA/LPS/IFA Promotes IL-12p40 Production by DCSIGN DCs and Is Produced alongside CXCR3 Ligands in the IFR

(A) IL-12p40-YFP reporter mice were immunized as indicated, and dLNs were harvested 72 h later. Shown are representative flow cytometry plotsand frequency of IL12-YFP$^+$ cells within CD11c$^+$ DCs (top) and DCSIGN DCs within IL12-YFP$^+$ DCs (bottom). Results are pooled from four independent experiments (n = 7–12 mice per group).

(B) WT or IL12b$^{-/-}$ mice were immunized, and dLNs were harvested 6 days later. Total dLN cells were cultured with OVA for 3 days and analyzed for IFNγ in supernatants by ELISA (top) and for Th1 differentiation by ICS as in Figure 1. Results are pooled from two

independent experiments (n = 2–8 mice per group).(C) dLNs from REX3/IL12-YFP reporter mice 72 h post-OVA/LPS/IFA immunization were stained with CD19and analyzed by confocal microscopy (CD19, gray; CXCL9-RFP, red; CXCL10-BFP, blue; IL12p40-YFP, green). Merge (left), individual channels (right), and zoom of the highlighted IFR (bottom). Representative image from four independent experiments (n = 8 LNs).

(D) WT or CCR7$^{-/-}$ mice were immunized, an dLNs were harvested 72 h later. Cell counts of indicated cell subsets. Results are pooled from three independent experiments (n = 6–10 mice per group).

Data are presented as mean ± SEM. *p ≤ 0.05, **p ≤ 0.01, ****p ≤ 0.0001.

KEY RESOURCES TABLE

REAGENT or RESOURCE	SOURCE	IDENTIFIER
FITC anti-mouse Ly6G (1A8)	BioLegend	Cat# 127606; RRID: AB_1236494
PerCP/Cy5.5 anti-mouse Ly6G (1A8)	BioLegend	Cat# 127616; RRID: AB_1877271
PE anti-CCR2 (475301)	R&D Systems	Cat# FAB5538P; RRID: AB_10718414
AF700 anti-CCR2 (475301)	R&D Systems	Cat# FAB5538N; RRID: AB_2725739
PE/Cy7 anti-mouse CD8α (53-6.7)	BioLegend	Cat# 100722; RRID: AB_312761
Alexa Fluor 700 anti-mouse CD8α (53-6.7)	BioLegend	Cat# 100730; RRID: AB_493703
Brilliant Violet 786 anti-mouse CD8α (53-6.7)	BD Biosciences	Cat# 563332; RRID: AB_2721167
PE/Cy7 anti-rat CD90.1 (Thy-1.1) (OX-7)	BioLegend	Cat# 202518; RRID: AB_1659223
Brilliant Violet 605 anti-mouse CD11c (N418)	BioLegend	Cat# 117334; RRID: AB_2562415
Brilliant Violet 605 anti-mouse CD4 (GK1.5)	BioLegend	Cat# 100451; RRID: AB_2564591
Brilliant Violet 421 anti-mouse Ly6C (HK1.4)	BioLegend	Cat# 128032; RRID: AB_2562178
PerCP/Cy5.5 anti-mouse Ly6C (HK1.4)	BioLegend	Cat# 128012; RRID: AB_1659241
Brilliant Violet 421 anti-mouse IFNγ (XMG1.2)	BioLegend	Cat# 505830; RRID: AB_2563105
Brilliant Violet 786 anti-mouse IFNγ (XMG1.2)	BioLegend	Cat# 563773; RRID: AB_2738419
eFluor660 anti-mouse CD209a (DCSIGN) (MMD3)	ThermoFisher Scientific	Cat# 50-2094-82; RRID: AB_11219065
APC anti-mouse TNFα (MP6-XT22)	BioLegend	Cat# 506308; RRID: AB_315429
APC/Cy7 anti-mouse I-A/I-E (M5/114.15.2)	BioLegend	Cat# 107628; RRID: AB_2069377
Brilliant Violet 711 anti-mouse F4/80 (BM8)	BioLegend	Cat# 123147; RRID: AB_2564588
Brilliant Ultraviolet 737 anti-mouse CD11b (M1/70)	BD Biosciences	Cat# 564443; RRID: AB_2738811
Brilliant Ultraviolet 395 anti-mouse CD90.2 (Thy-1.2)	BD Biosciences	Cat# 565257; RRID: AB_2739136
Brilliant Ultraviolet 395 anti-mouse NK1.1 (PK136)	BD Biosciences	Cat# 564144; RRID: AB_2738618
Brilliant Ultraviolet 395 anti-mouse CD19 (1D3)	BD Biosciences	Cat# 563557; RRID: AB_2722495
Brilliant Ultraviolet 395 anti-mouse CD3 (145-2C11)	BD Biosciences	Cat# 563565; RRID: AB_2738278
eFluor780 Fixable Viability Dye	ThermoFisher Scientific	Cat# 65-0865-18
Alexa Fluor 488 anti-mouse/human CD45R/B220 (RA3-6B2)	BioLegend	Cat# 103225; RRID: AB_389308
Alexa Fluor 647 anti-mouse/human CD45R/B220 (RA3-6B2)	BioLegend	Cat# 103226; RRID: AB_389330
Alexa Fluor 647 anti-mouse CD169 (3D6.112)	BioLegend	Cat# 142408; RRID: AB_2563621
Biotinylated anti-mouse CD290b (SIGNR1) (polyclonal)	R&D Systems	Cat# BAF1836; RRID: AB_2074454
Brilliant Violet 421 Streptavidin	BioLegend	Cat# 405226
Purified anti-mouse CD21/35 (7G6)	BD Biosciences	Cat# 553817; RRID: AB_395069
Purified anti-mouse PNAd (MECA-79)	BD Biosciences	Cat# 553863; RRID: AB_395099
LEAF purified anti-mouse CD28 (37.51)	BioLegend	Cat# 102112; RRID: AB_312877
Goat anti-mouse IgG1-HRP, human adsorbed	Southern Biotech	Cat# 1070-05; RRID: AB_2650509
Goat anti-mouse IgG2-HRP, human adsorbed	Southern Biotech	Cat# 1080-05; RRID: AB_2734756
InVivoMab anti-mouse Ly6G/Ly6C (Gr1) (RB6-8C5)	Bio X Cell	Cat# BE0075; RRID: AB_10312146
InVivoMab mouse IgG2b isotype control (MPC-11)	Bio X Cell	Cat# BE0086; RRID: AB_1107791
TruStain FcX anti-mouse CD16/32 (93)	BioLegend	Cat# 101320; RRID: AB_1574975

REAGENT or RESOURCE	SOURCE	IDENTIFIER
Normal Goat Serum	Jackson ImmunoResearch	Cat# 005-000-121; RRID: AB_2336990
Chemicals, Peptides, and Recombinant Proteins		
Ovalbumin	Sigma-Aldrich	Cat# A5503
OVA peptide (323-339)	InvivoGen	Cat# vac-isq
PMA	Sigma-Aldrich	Cat# P1585
Ionomycin calcium salt from Streptomyces conglobatus	Sigma-Aldrich	Cat# I0634
Brefeldin A Solution	BioLegend	Cat# 420601
DNase I, grade II	Sigma-Aldrich	Cat# 10104159001
Liberase DH	Sigma-Aldrich	Cat# 5401054001
Lipopolysaccharide	InvivoGen	Cat# tlrl-eklps
FTY720 (Fingolimod)	Cayman Chemicals	Cat# 10006292
Diphtheria Toxin from *Corynebacterium diphtheriae*	Sigma-Aldrich	Cat# D0564-1 MG
OCT Compound	Tissue-Tek	Cat# 4583
TRIzol Reagent	Thermo Fisher Scientific	Cat# 15596018
MultiScribe Reverse Transcriptase	Thermo Fisher Scientific	Cat# 4311235
GeneAMP dNTP mix with dTTP	Thermo Fisher Scientific	Cat# N8080260
MgCl2 Solution 25 mM	Thermo Fisher Scientific	Cat# 4486224
10x PCR Buffer II	Thermo Fisher Scientific	Cat# 4486220
Oligio d(T)16	Thermo Fisher Scientific	Cat# 100023441
Random Hexamers 50 mM	Thermo Fisher Scientific	Cat# 100026484
RNase Inhibitor	Thermo Fisher Scientific	Cat# 100021540
FastStart Essential DNA Green Master	Roche	Cat# 25595200
Incomplete Freund's Adjuvant	Sigma-Aldrich	Cat# F5506
AddaVax	InvivoGen	Cat# vac-adx-10
1-step Ultra TMB_ELISA Solution	ThermoFisher Scientific	Cat# 34028
Nonfat-Dried Milk, bovine	Sigma-Aldrich	Cat# M7409
Intracellular Fixation & Permeabilization Buffer Set	ThermoFisher Scientific	Cat# 88-8824-00
ProLong Diamond Antifade Mountant	ThermoFisher Scientific	Cat# P36961
Critical Commercial Assays		
Mouse IFNγ ELISA MAX Standard	BioLegend	Cat# 430803
EasySep Mouse $CD4^+CD62L^+$ T Cell Isolation Kit	Stemcell	Cat# 18765
EasySep Mouse Monocyte Isolation Kit	Stemcell	Cat# 19861
CountBright Absolute Counting Beads	ThermoFisher Scientific	Cat# C36950
Alexa Fluor 488 Protein Labeling Kit	ThermoFisher Scientific	Cat# A10235
Alexa Fluor 594 Microscale Protein Labeling Kit	ThermoFisher Scientific	Cat# A30008
Alexa Fluor 647 Microscale Protein Labeling Kit	ThermoFisher Scientific	Cat# A30009
Experimental Models: Organisms/Strains		
Mouse: C57BL/6	Charles River Laboratory	Cat# 027
Mouse: B6.129(Cg)-Ccr2tm2.1Ifc/J	The Jackson Laboratory	Cat# 017586

REAGENT or RESOURCE	SOURCE	IDENTIFIER
Mouse: REX3-Tg	Groom et al., 2012	Cat# N/A
Mouse: C57BL/6-Tg(CAG-EGFP)131Osb/LeySopJ	The Jackson Laboratory	Cat# 006567
Mouse: B6.Cg-Tg(TcraTcrb)425Cbn/J (OT2m)	The Jackson Laboratory	Cat# 004194
Mouse: B6.PL-Thy1a/CyJ	The Jackson Laboratory	Cat# 000406
Mouse: B6.129P2-Lyz2tm1(cre)Ifo/J	The Jackson Laboratory	Cat# 004781
Mouse: C57BL/6-Tg(Csf1r-HBEGF/mCherry)1Mnz/J	The Jackson Laboratory	Cat# 024046
Mouse: B6.129-Il12btm1Lky/J	The Jackson Laboratory	Cat# 006412
Mouse: *Ifnar*$^{-/-}$	Müller et al., 1994	Cat# N/A
Mouse: B6.129S7-ifngr1tm1Agt/J	The Jackson Laboratory	Cat# 003288
Mouse: B6.129P2(C)-Ccr7tm1Rfor/J	The Jackson Laboratory	Cat# 006621
Mouse: B6.129S1-Il12b^{tm1Jm}/J	The Jackson Laboratory	Cat# 002693
Oligonucleotides		
mCcl2 FWD (5′-TTA AAA ACC TGG ATC GGA ACC AA-3′)	This paper	https://pga.mgh.harvard.edu/primerbank/
mCcl2 REV (5′-GCA TTA GCT TCA GAT TTA CGG GT-3′)	This paper	https://pga.mgh.harvard.edu/primerbank/
mCcl7 FWD (5′-GCT GCT TTC AGC ATC CAA GTG-3′)	This paper	https://pga.mgh.harvard.edu/primerbank/
mCcl7 REV (5′-CCA GGG ACA CCG ACT ACT G-3′)	This paper	https://pga.mgh.harvard.edu/primerbank/
mCcl12 FWD (5′-GCT GGA CCA GAT GCG GTG-3′)	This paper	https://pga.mgh.harvard.edu/primerbank/
mCcl12 REV (5′-CCG GAC GTG AAT CTT CTG-3′)	This paper	https://pga.mgh.harvard.edu/primerbank/
mGAPDH FWD (5′-GGC AAA TTC AAC GGC ACA GT-3′)	This paper	N/A
mGAPDH REV (5′-AGA TGG TGA TGG GCT TCC C-3′)	This paper	N/A
Software and Algorithms		
Prism v8	GraphPad	https://www.graphpad.com; RRID: SCR_002798
Zen Black 2012 v8	Zeiss	https://www.zeiss.com/microscopy/us/products/microscope-software/zen.html; RRID: SCR_013672
Imaris v8.3.1	Bitplane	https://imaris.oxinst.com/packages; RRID: SCR_007370
Softmax Pro	Molecular Devices	https://www.moleculardevices.com/products/microplate-readers/acquisition-and-analysis-software/softmax-pro-software; RRID: SCR_014240
BD FACS Diva v8	BD Biosciences	https://www.bdbiosciences.com/us/instruments/clinical/software/flow-cytometry-acquisition/bd-facsdiva-software/m/333333/overview; RRID: SCR_001456
FlowJo v10	Tree Star	https://www.flowjo.com/solutions/flowjo/downloads; RRID: SCR_008520